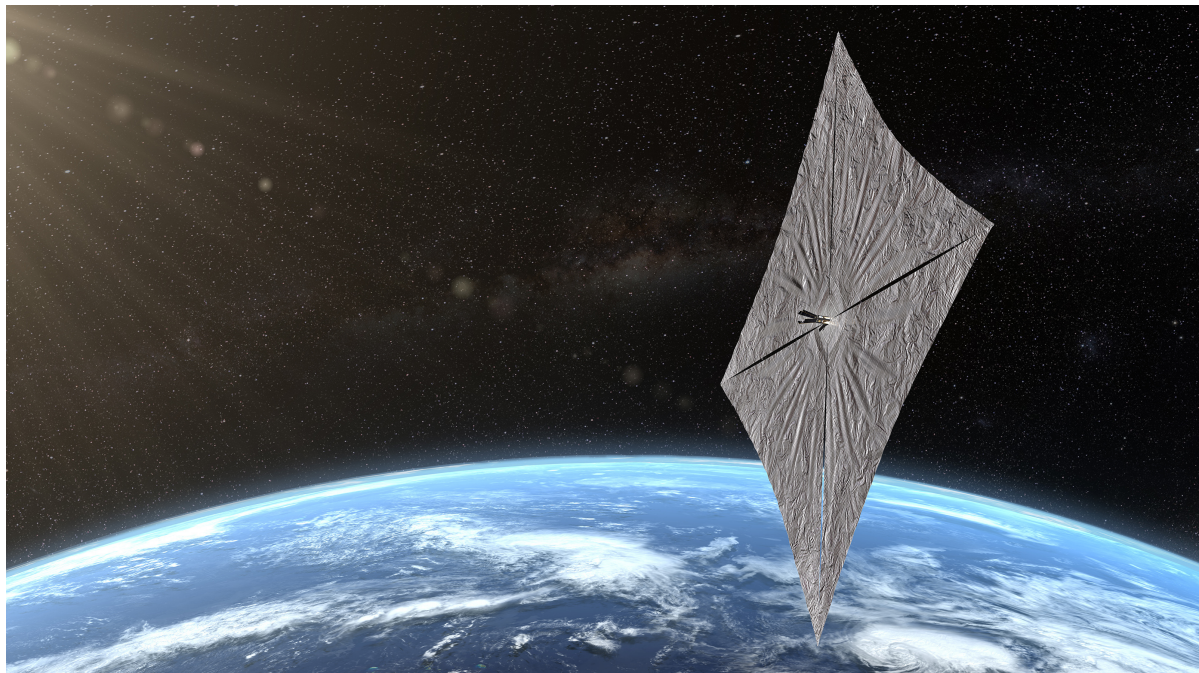


SATELLITE DYNAMICS AND ATTITUDE CONTROL

Max Newport, Valerie Pietrasz

06 April 2021



REVISION HISTORY

| VERSION | REVISION NOTES |
|---------|--|
| PS1 | <ul style="list-style-type: none">- Created document- Added PS1 material: Mission specifications, satellite selection.- Structure and mass distribution. Inertia matrix, body axes. Orbit. |
| PS2 | <ul style="list-style-type: none">- Added PS2 material: Euler propagator, validation, axisymmetry.- Modified inertia to include asymmetric components (in PS1 and Appendix). |
| PS3 | <ul style="list-style-type: none">- Added PS3 material: attitude propagation, integration, stability and equilibrium tests.- Added appendix for comparison of Euler 312 and quaternion results. |
| PS4 | <ul style="list-style-type: none">- Added PS4 material: dual spin, gravity gradient.- Added comparison of quaternion vs. 312 Euler integration, along with error in appendix. |

Table 1: Summary of project revisions.

TABLE OF CONTENTS

| | | |
|----------|---|-----------|
| 1 | INTRODUCTION | 4 |
| 2 | PROBLEM SET 1 | 4 |
| 2.1 | MISSION ADCS CHARACTERISTICS | 4 |
| 2.2 | SIMILAR MISSIONS | 5 |
| 2.3 | MECHANICAL LAYOUT | 6 |
| 2.4 | INERTIA PROPERTIES | 7 |
| 2.5 | OUTER SURFACE DISCRETIZATION | 7 |
| 2.6 | ORBITAL ELEMENTS & PROPAGATION | 8 |
| 3 | PROBLEM SET 2 | 9 |
| 3.1 | PRINCIPAL AXES | 9 |
| 3.2 | NO-TORQUE PROPAGATION | 11 |
| 3.3 | AXIAL SYMMETRY | 13 |
| 4 | PROBLEM SET 3 | 14 |
| 4.1 | KINEMATIC INTEGRATION | 14 |
| 4.2 | ATTITUDE PROPAGATION | 16 |
| 4.3 | EQUILIBRIUM TESTS | 17 |
| 4.4 | STABILITY TESTS | 17 |
| 5 | PROBLEM SET 4 | 18 |
| 5.1 | DUAL SPIN | 18 |
| 5.2 | GRAVITY GRADIENT TORQUE | 20 |
| 6 | REFERENCES | 21 |
| | Appendices | 23 |
| A | Mass Distribution Analysis | 23 |
| A.1 | Solar Sail | 23 |
| A.2 | Sail Booms | 24 |
| A.3 | Forward Body | 24 |
| A.4 | Solar Panels | 25 |
| A.5 | Rear Body | 25 |
| B | LS2 System Drawings | 26 |
| C | VBA Solidworks Macro for Exporting Surface Normals | 27 |
| D | Verification of Inertia Computations | 29 |
| E | Additional Orbital Propagator Notes | 31 |
| F | Quaternion and 312 Euler Kinematic Comparison | 31 |
| G | Dual Spin Equilibrium & Stability Analysis | 31 |

1 INTRODUCTION

We have chosen to study the LightSail 2 mission (LS2), a solar sailing proof-of-concept mission developed by The Planetary Society. Solar sails use solar radiation pressure (SRP) to propel the spacecraft, and JAXA's IKAROS mission in 2021 was the first mission to successfully do so in interplanetary space. In contrast, LS2 used solar sailing in Earth orbit to perform a controlled orbital maneuver; namely, raising spacecraft apogee.

2 PROBLEM SET 1

2.1 MISSION ADCS CHARACTERISTICS

We will model LightSail 2's mission objectives and hardware. The spacecraft was deployed into a circular, low-earth orbit at 720km altitude, 24 degrees inclination, where it then attempted to raise its apogee using solar sailing. For analysis, we will use the starting orbital parameters with arbitrary values selected for the unknown parameters, as noted in the orbital elements section.

The method by which LS2 raised its apogee is called the on/off control strategy. While the spacecraft was moving away from the sun, the sail normal vector pointed toward the sun ("on") in order to increase spacecraft velocity. While the spacecraft was moving toward the sun, the spacecraft normal pointed perpendicularly to the direction of the sun ("off"), to maintain orbit until the spacecraft was once again moving away from the sun. Thus, the spacecraft had two target attitudes: sun pointing and sun-perpendicular pointing. *The spacecraft attitude will be represented in this project using quaternions.*

In order to realize sun and sun-perpendicular pointing, the spacecraft will require at minimum sun sensors, but additional sensors for accuracy improvement and redundancy would be preferred. To move between the two target attitudes will require 90 degree slew maneuvers twice per orbit, which can be achieved with a variety of actuators. In this case, torque rods and momentum wheels were used.

The high level ADCS requirements are listed below [6]. To keep the project within a reasonable scope, we will focus on those above the line. Anything below the line will be assumed to be met.

- Provide attitude knowledge to within 5 degrees per axis during all mission phases.
- Sun sensors provide data on the angle of light incidence to the sensors to within ± 3 degrees accuracy.
- Magnetometers provide attitude knowledge of the body-fixed x-, y-, and z-axes to within ± 5 degrees relative to the Earth magnetic field.
- Utilize a momentum wheel to achieve 90-degree slew maneuvers about one axis in < 5 minutes.
- Following solar sail deployment, be capable of providing an angular acceleration of 0.0005 degrees/sec² per axis.
- Detumble from a maximum of 10 degrees per second per axis after sail deployment.
- Align +Z axis of the spacecraft with the magnetic field with maximum variation once settled of < 60 degrees.

| Component | Number | Specifications |
|---------------|--------|---------------------------|
| Sun sensors | 5 | Max error: 3 degrees |
| Magnetometers | 4 | Max error: 5 degrees |
| Primary Gyro | 1 | Max error: 3 degrees/axis |
| Intrepid Gyro | 1 | Max error: 3 degrees/axis |

Table 2: LS2 Sensors

| Component | Number | Specifications |
|----------------|--------|---|
| Torque Rods | 3 | Max torque: $1 \text{ Am}^2 \times \vec{B}$ |
| Momentum Wheel | 1 | Max torque: 0.06 Nm^2 |

Table 3: LS2 Actuators

- Damp attitude rates within 2 hours of P-POD deployment.
- Accommodate a tip off rate of up to 25 degree/sec per axis from P-POD deployment.
- Prior to sail deployment, utilize torque rods to achieve attitude control to within 10 degree per axis.
- Prior to sail deployment, be capable of providing an angular acceleration of 0.1 degrees/s^2 per axis.
- Prior to solar sail deployment, provide attitude control to within 10 degrees per axis.
- Downlink telemetry for sensors, actuators and performance data.
- Sample spacecraft angular rates using gyro sensors.
- Be actively controllable in each of its three-axes.

To achieve these objectives, LS2 used the sensors and actuators listed in Tables 3 and 2. These components were selected for their low cost, low mass, and reliability.

2.2 SIMILAR MISSIONS

There are several satellites with similar mission objectives. LightSail 1 (LS1) was originally developed to meet the same objective, but was down-scoped to only achieve the goals listed prior to and including sail deployment. To reduce development costs, LS2 reused much of the LS1 design. Notable differences include a lower orbital altitude (400km for LS1 compared to 720km for LS2), removing the momentum wheel to simplify the spacecraft and reduce costs, and a simpler ADCS on LS1 [3].

IKAROS, the first successful solar sail mission, differed from LS2 in three major respects: first, it orbits the sun rather than Earth, and thus must survive the interplanetary, rather than near-Earth, environment. Secondly, it performs attitude control using liquid crystals in the sail that alter the diffusivity and reflectivity of the solar sail to allow for differential SRP across the sail [9]. Lastly, while LS1 and 2 used rigid booms to maintain the sail's shape, IKAROS removed these to save mass, and thus relies on centrifugal force from spacecraft spin to keep the sail extended. All of these differences have driven ADCS requirements that are different from LS2 (such as maintaining a minimum spin about the axis normal to the sail).

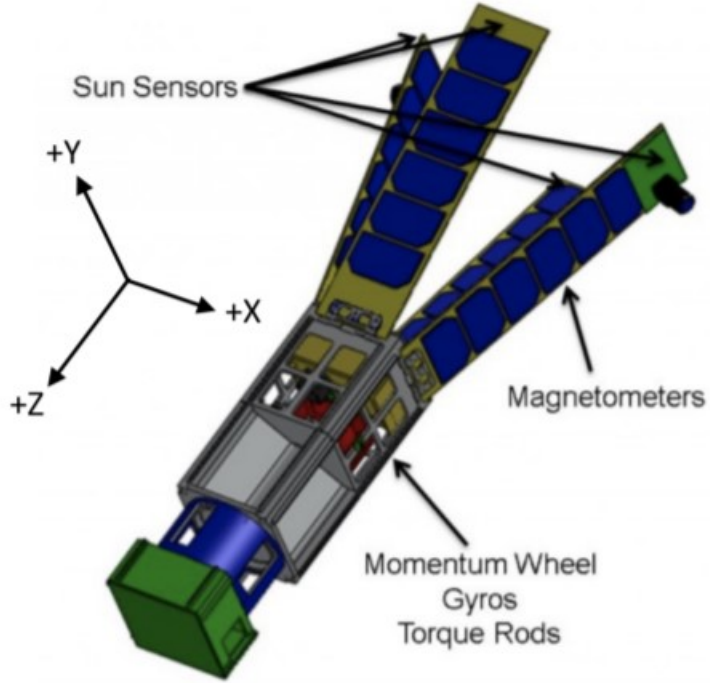


Figure 1: Annotated Full-Detail Layout of 3U Structure

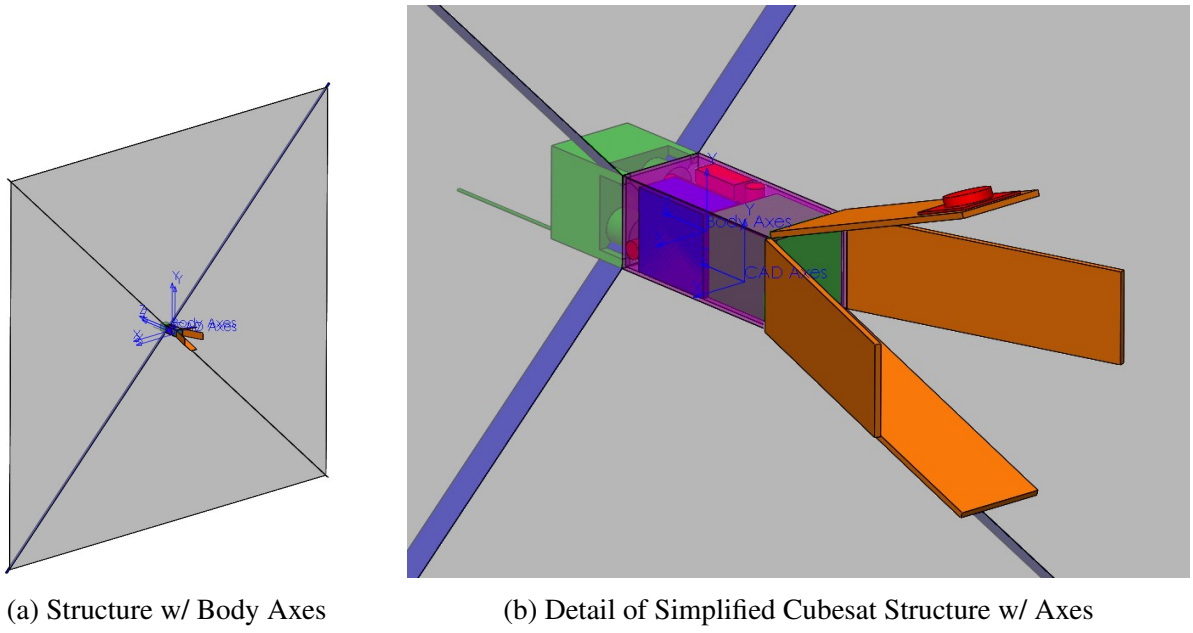
NASA has launched missions similar to LS1 and LS2, NanoSail-D, to prove usage of solar sails as passive de-orbiting mechanisms. The first NanoSail-D was lost in launch, while the second performed many of the desired functions, de-orbiting after 240 days [2].

Another relevant mission is Prox-1, LS2's launch partner. Originally developed to demonstrate automated, close-proximity maneuvers relative to another CubeSat (with LS2 as its target), the proximity maneuvers were ultimately cut and the spacecraft now serves primarily to monitor and image LS2. Prox-1's ADCS mission requirements are very different (and more strict) than LS2's, requiring greater attitude knowledge and control to perform its maneuvers and imaging [7].

2.3 MECHANICAL LAYOUT

High-level drawings of the LS2 system in its various configurations are provided in Appendix B; note that this study will only consider the LIGHTSAIL DEPLOYED configuration. The basic layout of the 3U structure with the placement of primary ACDS components is provided in Figure 1. The body coordinates used to describe the mechanical layout are plotted in Figure 2. Note that the system is roughly axisymmetric over the x and y , with the $+z$ axis pointing away from the deployed solar panels.

LS2 uses a motorized TRAC (Triangular Roll-able And Collapsible) boom deployment system to unfurl its 5.57m square Mylar sail. During launch, the 4 primary solar panels are folded along the length of the satellite - once deployed, the panels extend along the $-z$ axis. After de-tumbling with magnetic torquing, the booms extend and unfold the 4.5 micron thick Mylar from a central "sail housing" unit. Due to limited knowledge about the exact mass distribution of the satellite and a desire for a simplified model, the mechanical layout has been reduced to five primary components, detailed in Table 4 below. The mass calculations are described in



(a) Structure w/ Body Axes

(b) Detail of Simplified Cubesat Structure w/ Axes

Figure 2: Simplified Mechanical Layout of LightSail 2

| Name | Color in 3D Model | Subsystems | Mass (kg) |
|--------------|-------------------|--|-------------|
| Forward Body | Green | Comms, Boom Motors (x2), Boom Housing | 1.47 |
| Booms | Blue | TRAC Booms (x4) | 0.93 |
| Solar Sail | Grey | Mylar sail | 0.20 |
| Rear Body | Purple | Magnotorquers, Mom. Wheel, Power, Avionics | 1.73 |
| Solar Panels | Orange | Solar Cells, Magnetometers, Cameras | 0.60 |
| TOTAL | - | - | 4.93 |

Table 4: Primary Components of Simplified Mechanical Layout

further detail in Appendix A; while some effort was taken to include asymmetric contributions to the total volume, the large contribution of the square solar sail creates a fairly axisymmetric system.

2.4 INERTIA PROPERTIES

The inertia properties provided below were computed using the 3D model shown in Figure 2. An analytical verification of these values is provided in Appendix D. Along the principal axes, the moments of the inertia for the system are

$$I_{xx} = 3.10288 \text{ kg} \cdot \text{m}^2, I_{yy} = 3.10553 \text{ kg} \cdot \text{m}^2, I_{zz} = 5.98305 \text{ kg} \cdot \text{m}^2$$

Using our 3D model to calculate the full inertia matrix yields, in the body frame,

$$L = \begin{bmatrix} 3.10553 & -0.00011 & -0.00003 \\ -0.00011 & 3.10289 & -0.00005 \\ -0.00003 & -0.00005 & 5.98305 \end{bmatrix} \text{ kg} \cdot \text{m}^2$$

2.5 OUTER SURFACE DISCRETIZATION

To provide an easy way of analyzing environmental perturbative torques, we also simplify the outer geometry. The surface normals and centroids are pulled from the CAD model, where the

solar panels and solar sail are taken to have a negligible thickness (effectively reducing those components to planes) and minor elements like cameras are not included in the discretization. Using a Solidworks VBA Macro, we export the centroid, unit normal, and area information for each outward-facing surface of interest. The MATLAB script below imports the information into MATLAB data structures for use in future simulations. Table 5 displays the centroid locations in body coordinates, the associated normal vector, and the associated area.

```

1 %% get_surfacedata()
2 % Reads surface data from CSV file.
3 % No input.
4 % Output:
5 %   - C : an (n x 3) matrix, where n is the number of surfaces, denoting
6 %         the location in body coordinates of each surface's ...
7 %         centroid in m.
8 %   - N : an (n x 3) matrix denoting the unit outward-facing normal for
9 %         each surface.
10 %   - A : an (n x 1) matrix denoting the area for each surface, in m^2.
11
12 function [C, N, A] = get_surfacedata()
13     centroid_file = 'CentroidData.csv';
14     data = readtable(centroid_file, 'ReadVariableNames', false);
15     C = [data.Var1 , data.Var2 , data.Var3];
16     N = [data.Var4 , data.Var5 , data.Var6];
17     A = data.Var7;
18 end

```

| Location (m) | Normal Vec | Area (m ²) |
|--------------------------|--------------------|------------------------|
| (-0.003, -0.054, -0.049) | (0, -1, 0) | 0.023 |
| (0.047, -0.004, -0.049) | (1, 0, 0) | 0.023 |
| (-0.003, 0.046, -0.049) | (0, 1, 0) | 0.023 |
| (-0.053, -0.004, -0.049) | (-1, 0, 0) | 0.023 |
| (-0.003, -0.004, -0.164) | (0, 0, -1) | 0.01 |
| (-0.003, 0.1, -0.313) | (0, -0.94, -0.342) | 0.032 |
| (0.101, -0.004, -0.313) | (-0.94, 0, -0.342) | 0.032 |
| (-0.003, -0.108, -0.313) | (0, 0.94, -0.342) | 0.032 |
| (-0.107, -0.004, -0.313) | (0.94, 0, -0.342) | 0.032 |
| (-0.003, 0.1, -0.313) | (0, 0.94, 0.342) | 0.032 |
| (-0.107, -0.004, -0.313) | (-0.94, 0, 0.342) | 0.032 |
| (-0.003, -0.108, -0.313) | (0, -0.94, 0.342) | 0.032 |
| (0.101, -0.004, -0.313) | (0.94, 0, 0.342) | 0.032 |
| (-0.053, -0.004, 0.121) | (-1, 0, 0) | 0.011 |
| (-0.003, -0.054, 0.121) | (0, -1, 0) | 0.011 |
| (0.047, -0.004, 0.121) | (1, 0, 0) | 0.011 |
| (-0.003, 0.046, 0.121) | (0, 1, 0) | 0.011 |
| (-0.003, -0.004, 0.176) | (0, 0, 1) | 0.01 |
| (-0.003, -0.004, 0.066) | (0, 0, -1) | 31.003 |
| (-0.003, -0.004, 0.066) | (0, 0, 1) | 31.003 |

Table 5: Centroid, normal, and area data pulled from CAD model.

2.6 ORBITAL ELEMENTS & PROPAGATION

The initial orbit propagator was developed for AA 279A in Winter 2019, and later further supplemented to include simple orbital perturbations (namely, atmospheric drag and J2, with

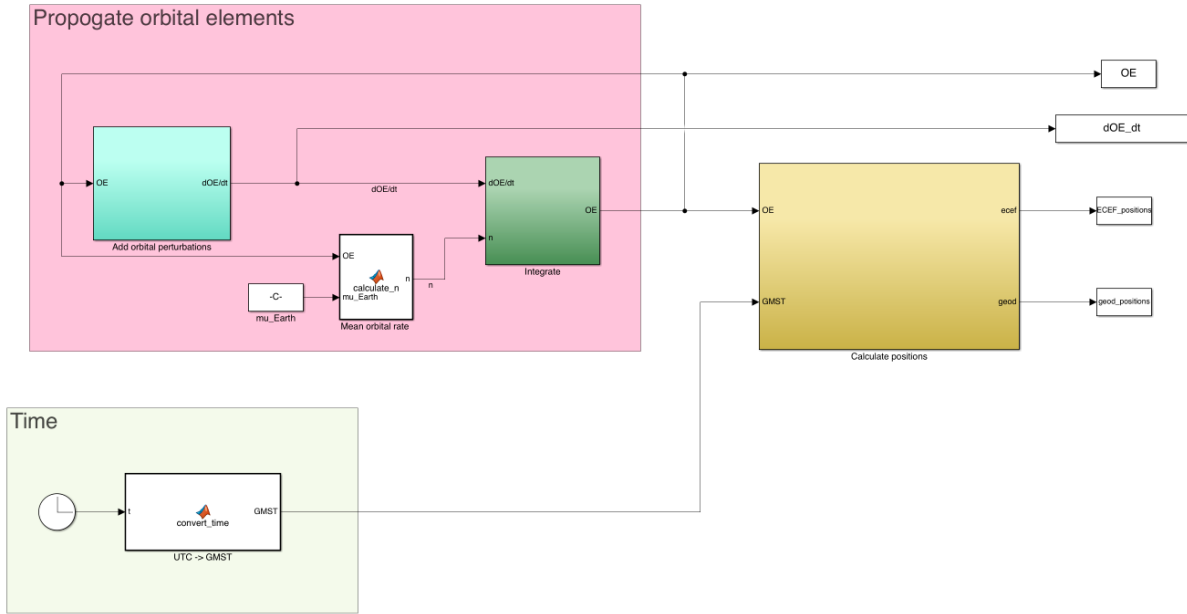


Figure 3: Top-level overview of the initial orbit propagator.

the infrastructure in place to add additional perturbations as relevant). SRP will be added to model the change in apogee that is one of the mission objectives. It will be incorporated into the ADCS simulation, and an overview is presented in Figure 3.

Initial values for the orbital elements are given in Table 6. These were used to produce the sample orbits given in Figure 4.

| Orbital element | Symbol | Initial value | Units | Notes |
|-----------------------|----------|---------------|-------------|---------------------------|
| Epoch | t_0 | 2019-07-08.20 | YY-MM-DD.dd | |
| Semi-major axis | a | 7095.553 | km | $R_E + 717.4175\text{km}$ |
| Eccentricity | e | 0.0010951 | | |
| Inclination | i | 24 | deg | |
| RAAN | Ω | 0 | deg | Selected arbitrarily |
| Argument of Periapsis | ω | 0 | deg | Selected arbitrarily |
| Eccentric anomaly | E | 0 | rad | Selected arbitrarily |

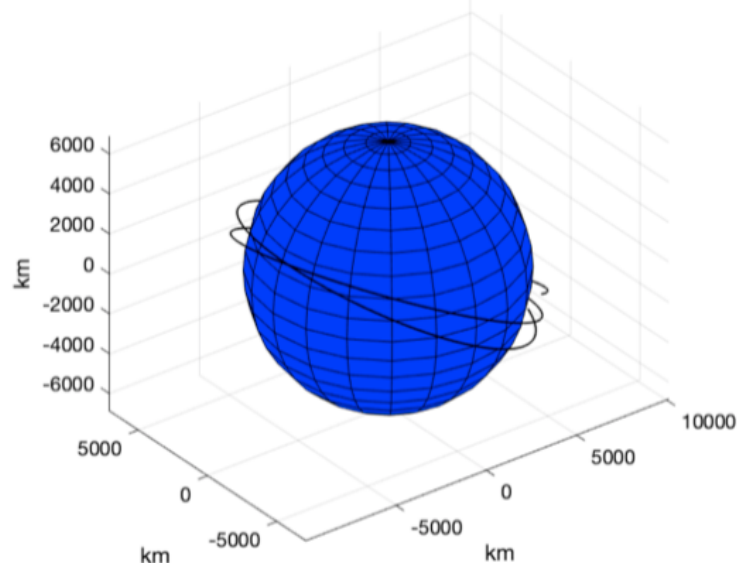
Table 6: Initial orbital elements, pulled from [8]. The arbitrarily selected values are those for which we do not have data, and have little effect on our modeling.

3 PROBLEM SET 2

3.1 PRINCIPAL AXES

The principal axes are shown alongside the body axes in Figure 5 - note that due to the overwhelming inertial contribution of the solar sail and booms, the primary difference between the axes systems is the flipping of the x and y axes to ensure well-ordered eigenvalues. Using the MATLAB script below, we can calculate the rotation matrix from the principal axes to body

Orbit of LS2 in ECEF reference frame



Groundtrack of LS2 in the Mercator lat/long projection

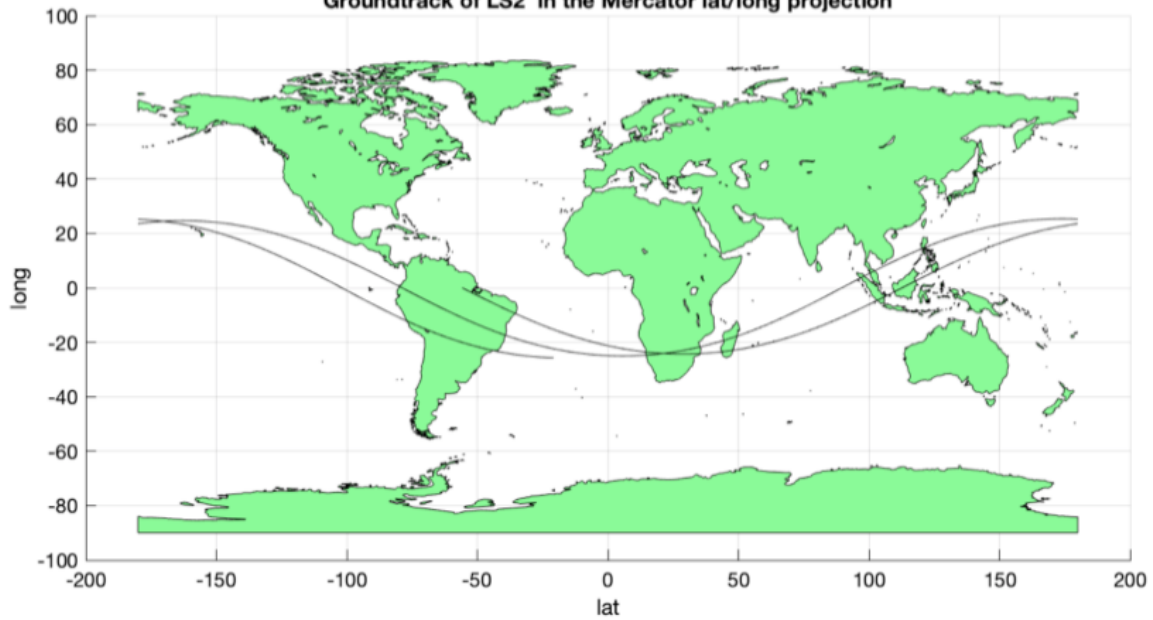


Figure 4: Initial sample orbits of LS2 given the orbital parameters in Table 6.

axes (whose columns represent the expression of the principal axes in body coordinates).

$$R = \begin{bmatrix} 0.04156 & 0.99911 & -1.042 \times 10^{-5} \\ 0.9991 & -0.04156 & -1.736 \times 10^{-5} \\ 1.778 \times 10^{-5} & 9.695 \times 10^{-6} & 1.000 \end{bmatrix}$$

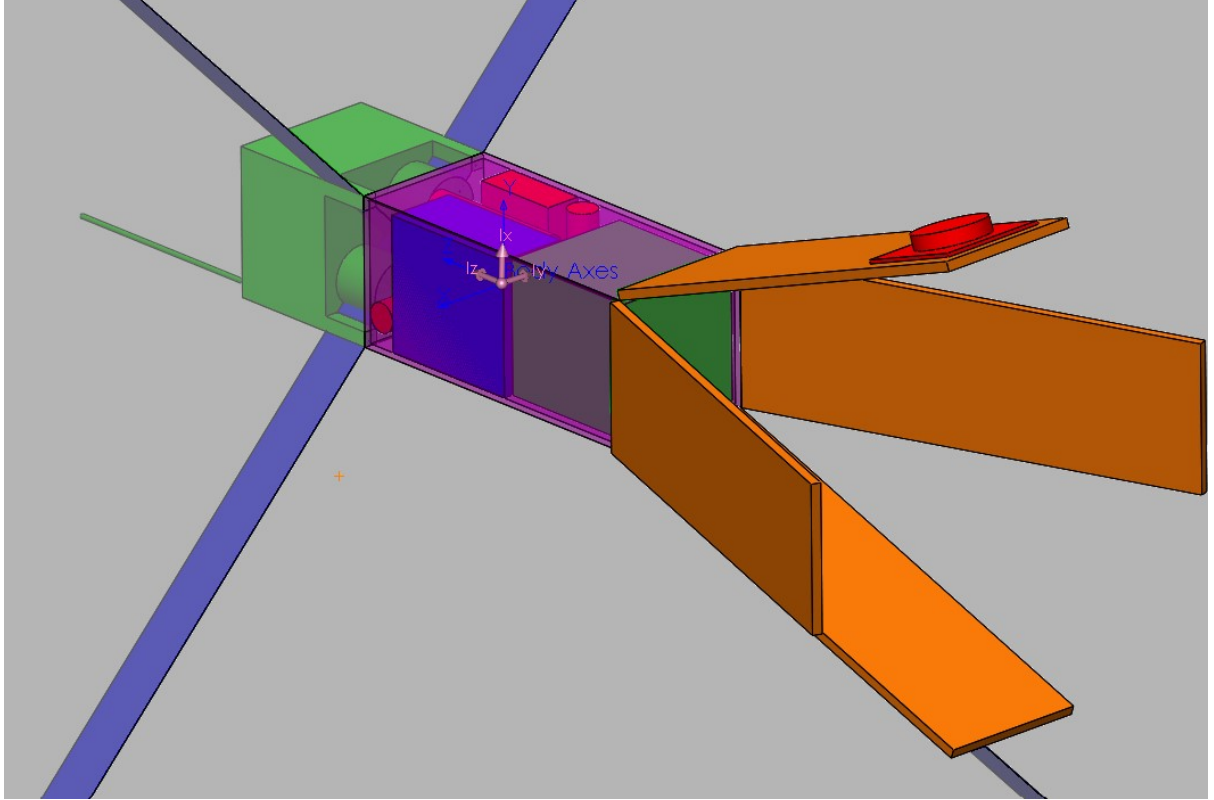


Figure 5: Body axes (blue) and principal inertia axes (pink), overlaying the simplified space-craft CAD model.

3.2 NO-TORQUE PROPAGATION

Using the Simulink block-diagram in Figure 6, we can propagate the angular velocity without the contribution of torque with respect to the principal axes. Plotting the resulting polhode over top of the momentum and energy ellipses that constrain the motion of the spacecraft in Figure 7, we can clearly see how our angular velocity vector is constrained to lay along the intersection of the two ellipses. Additionally, we can see from the planar projections of the polhode that while the x and z projections are (sections of) ellipses, the y projection is a hyperbola. Note that we use the following (arbitrary) initial angular velocity (expressed in principal axes) for our spacecraft:

$$\omega_0 = \begin{bmatrix} -6 \\ 8 \\ 0.1 \end{bmatrix} \text{ deg/sec}$$

To verify that our solution works in other cases, we consider an angular velocity along a principal axis to test out our propagator:

$$\omega_{0,2} = \begin{bmatrix} 0 \\ -10 \\ 0 \end{bmatrix} \text{ deg/sec}$$

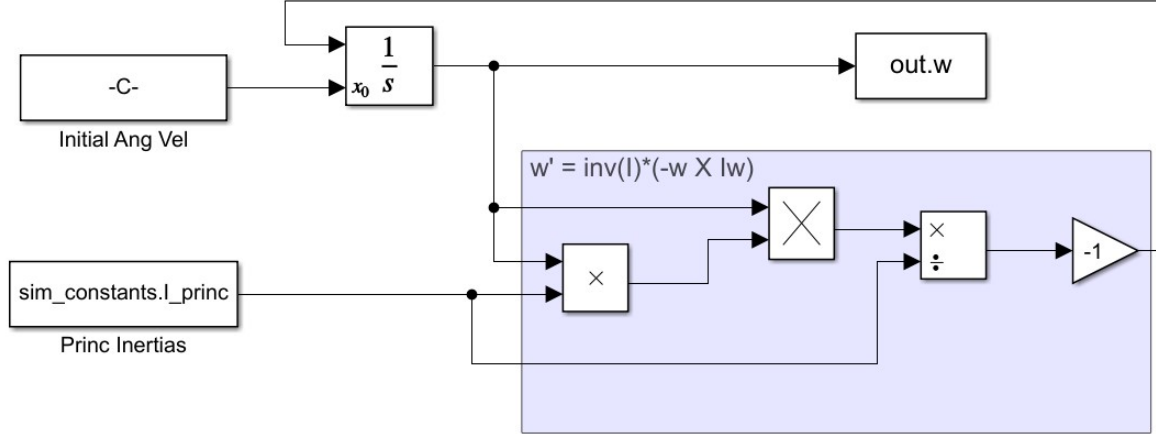


Figure 6: Simulink block diagram for propagating no-torque Euler equations in principal axes.

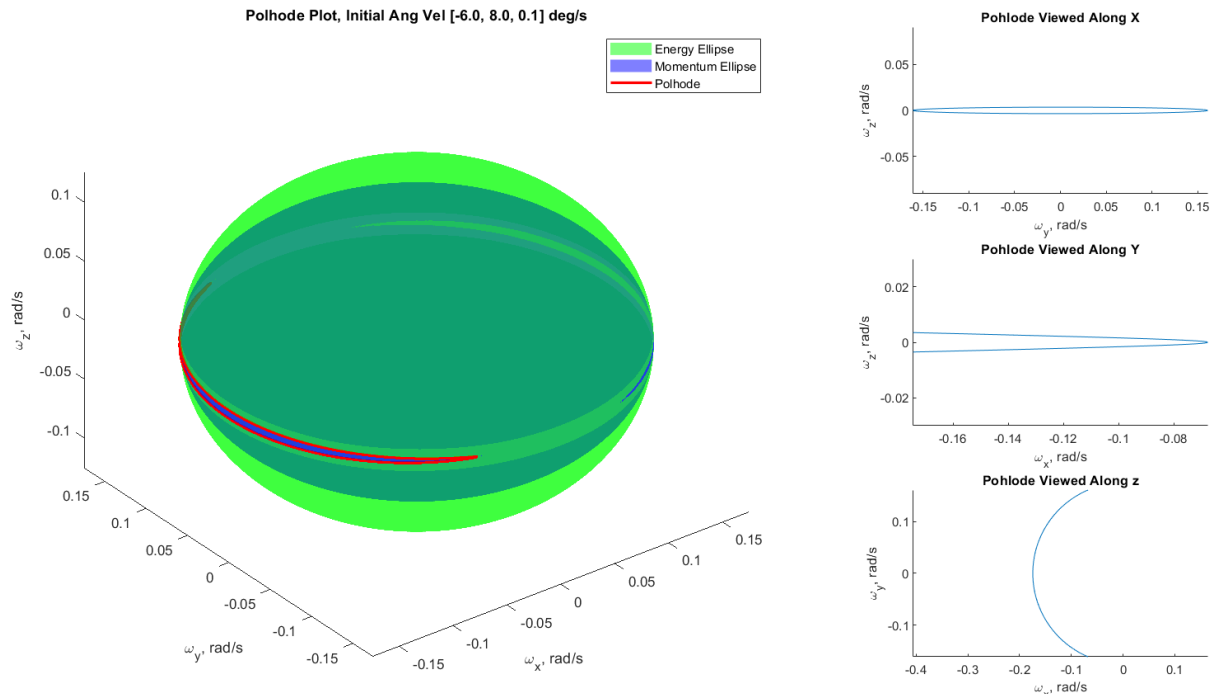


Figure 7: Plot of spacecraft polhode propagation in principal axes, assuming no-torque and non-trivial initial conditions.

The results of this propagation are shown in Figure 8. Again, our results are as expected - our angular velocity remains constant, but appears to lay at an unstable equilibrium (which makes sense, as our spin is about the intermediate axis - any off-axis angular velocity, however small, would result in tumbling).

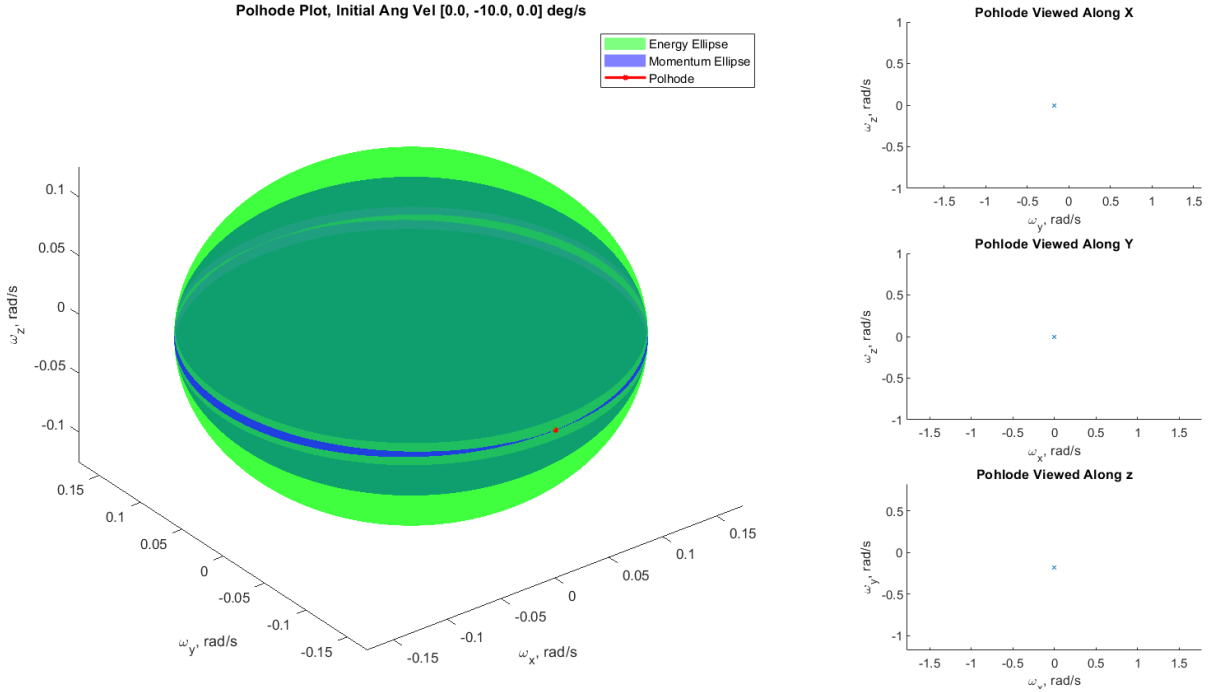


Figure 8: Plot of polhode propagation in principal axes, assuming no-torque and an initial angular velocity along the intermediate axis only.

3.3 AXIAL SYMMETRY

Although our spacecraft is nearly axisymmetric, we would like to analyze the case of torqueless true axial symmetry. For this, we set $I_{xx} = I_{yy} = 3.10288 \text{ kg} \cdot \text{m}^2$. The solution to Euler's equations in the axisymmetric case, where $\lambda = \frac{I_z - I_x}{I_x} \omega_z$, is simply the circle

$$\omega_{xy} = (\omega_{x0} + i\omega_{y0}) \exp(i\lambda t) \quad (1)$$

As usual for this representation of circles, ω_x is the real component while ω_y is the imaginary. Using the initial conditions that generated Figure 7, the analytic result across time is shown in Figure 9.

Comparing to the numeric results achieved using numeric propagation of the Euler equations, the error evolves as in Figure 10. First, we observe that there is no ω_z error. This is expected as in this system, it is constant and uncoupled from ω_x, ω_y , so there should be no numeric integration error. For ω_x, ω_y , the error starts small – on the order of 10^{-10} rad/s . The error behaves as sinusoids with mean 0 (and period similar to analytic result) bounded by exponential growth – the amplitudes are growing and will continue to grow unbounded as time progresses, although it will take many revolutions to reach any substantial error. Further, there is a phase delay between ω_x, ω_y in the numeric propagator.

Thus, within the integration error, the angular velocity vectors exchange momentum as expected, maintaining a constant ω_{xy} . However, there will be an apparent fluctuation of angular momentum about the mean due to integration error.

Finally, we compare the numeric results of the no-torque pseudo-axisymmetric case, as we have modelled the satellite, to the true axisymmetric case in Figure 11. Although the differences in inertia in the two cases are small ($I_{yy} = 3.10288 \text{ kg} \cdot \text{m}^2$ in the ideal case versus

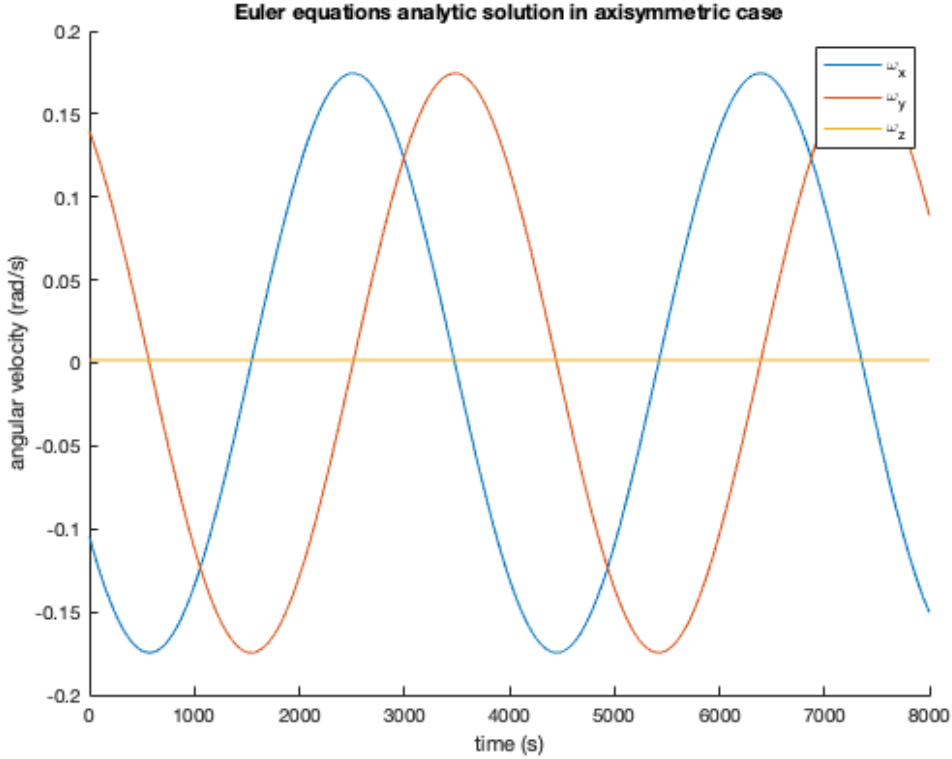


Figure 9: Time-domain solution of axisymmetric Euler equations using $\omega_0 = [-6, 8, 0.1]$.

$I_{yy} = 3.10553 \text{ kg} \cdot \text{m}^2$ in the real case), the error is not small for ω_x, ω_y . Because ω_z is largely decoupled and constant, this error is small, although noticeable. From this, we can see it is important for us to simulate the coupled motion of the nearly symmetric axes of our spacecraft and not make the true axisymmetric assumption.

4 PROBLEM SET 3

4.1 KINEMATIC INTEGRATION

To build toward an easily validated system, we build in kinematics integration that supports two types of attitude parameterization: quaternions (our primary method) and 312 Euler angles (a secondary method for validation). By toggling an input boolean, the simulation's attitude propagation can be switched between the two attitude parameterizations with ease.

The kinematics equation for quaternions was developed in class as

$$\frac{d\vec{q}}{dt} = \frac{1}{2}\Omega\vec{q}$$

for Ω as a function of the angular velocity, $\vec{\omega}$,

$$\Omega = \begin{bmatrix} 0 & \omega_z & -\omega_y & \omega_x \\ -\omega_z & 0 & \omega_x & \omega_y \\ \omega_y & -\omega_x & 0 & \omega_z \\ -\omega_x & -\omega_y & -\omega_z & 0 \end{bmatrix}$$

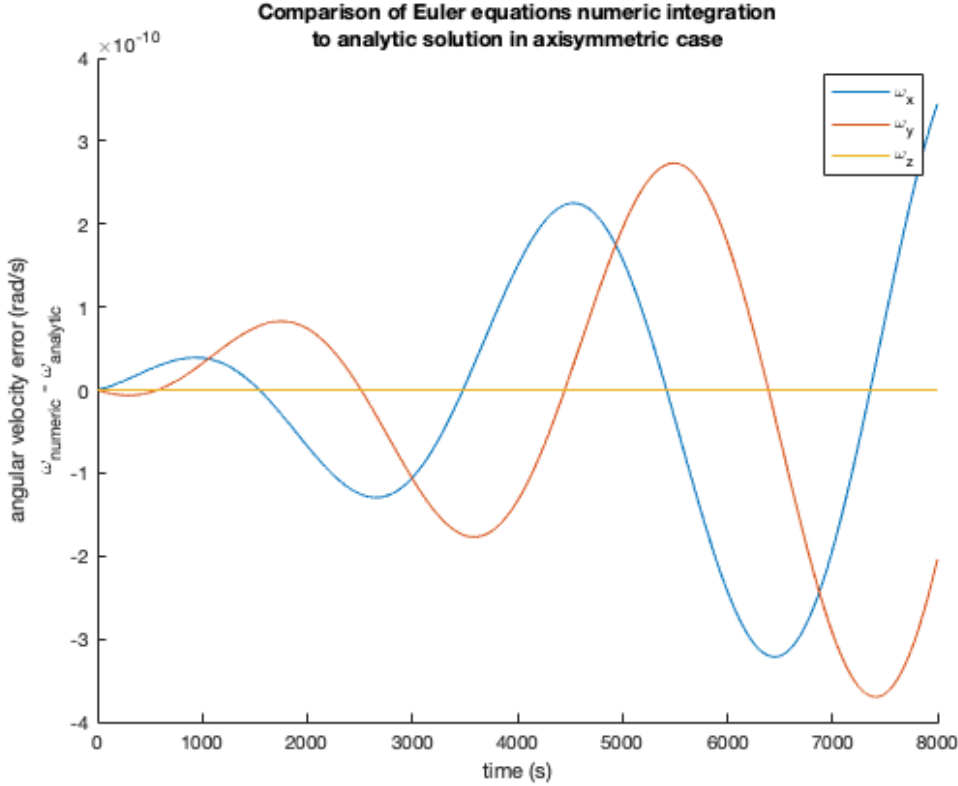


Figure 10: Evolution of error of numeric integration of Euler equations in the axisymmetric case ($\omega_0 = [-6, 8, 0.1]$.)

For 312 Euler angles, we derive the kinematics equation starting with the angular velocity in principal axes

$$\vec{\omega} = \dot{\phi}\hat{3} + \dot{\theta}\hat{1}' + \dot{\psi}\hat{y}$$

We get the components in principal frame by projecting onto the principal axes

$$\begin{aligned} \omega_x &= \vec{\omega} \cdot \hat{x} = \dot{\phi}(\hat{3} \cdot \hat{x}) + \dot{\theta}(\hat{1}' \cdot \hat{x}) \\ &= \dot{\phi} \cos \theta \sin \psi + \dot{\theta} \cos \psi \end{aligned}$$

$$\begin{aligned} \omega_y &= \vec{\omega} \cdot \hat{y} = \dot{\phi}(\hat{3} \cdot \hat{y}) + \dot{\theta}(\hat{1}' \cdot \hat{y}) + \dot{\psi} \\ &= \dot{\phi} \sin \theta + \dot{\psi} \end{aligned}$$

$$\begin{aligned} \omega_z &= \vec{\omega} \cdot \hat{z} = \dot{\phi}(\hat{3} \cdot \hat{z}) + \dot{\theta}(\hat{1}' \cdot \hat{z}) \\ &= \dot{\phi} \cos \theta \cos \psi - \dot{\theta} \sin \psi \end{aligned}$$

Solving for our angular rates, we get

$$\begin{aligned} \dot{\phi} &= \frac{1}{\cos \theta} (\omega_x \sin \psi + \omega_z \cos \psi) \\ \dot{\theta} &= \omega_x \cos \psi - \omega_z \sin \psi \\ \dot{\psi} &= \omega_y + \tan \theta (\omega_x \sin \psi + \omega_z \cos \psi) \end{aligned}$$

Note the singularity at $\theta = \frac{\pi}{2}$ for this parameterization.

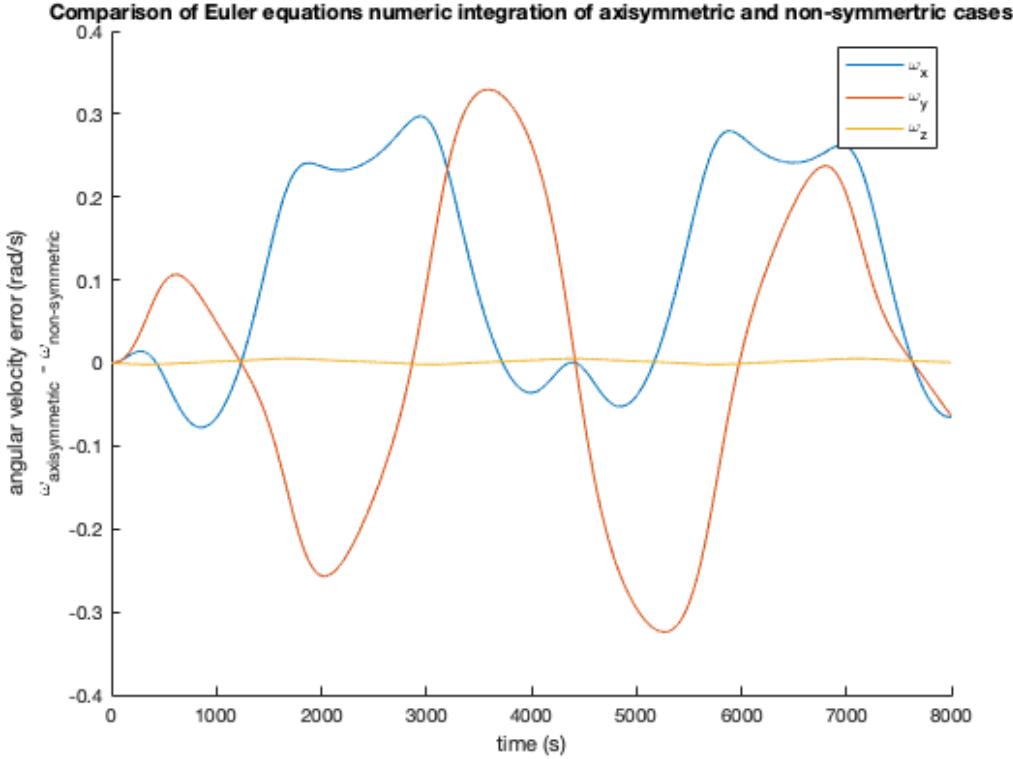


Figure 11: Evolution of difference between numeric integration of Euler equations in the pseudo-axisymmetric and true axisymmetric cases ($\omega_0 = [-6, 8, 0.1]$.)

Integrating our kinematics equations with the Euler equations from the previous problem set gives a full determination of our attitude in our orbital propagation. Using the bi-directional conversions between quaternions, 312 Euler angles, and direction cosine matrices, we can compare our solutions and visualize our attitude throughout the orbit. All solution below are generated using the quaternion kinematics, but a brief comparison with the 312 Euler results is provided in Appendix F.

4.2 ATTITUDE PROPAGATION

Given our previously-defined initial conditions, we propagate our spacecraft through a single orbit period. We can then verify that our simulated attitude and angular velocity match our expectations. In Fig 12, we can see that the components of angular momentum remain very nearly constant in the inertial frame throughout the duration of simulation (note that the small errors are due to numerical propagation effects). In Fig 13, we see that the angular velocity trace in inertial coordinates, the "herpolhode," lays in a plane normal to the (constant) angular momentum vector.

In Figs 14 and 15, we can see various coordinate systems of interest (RTN, body, and principal axes) plotted in time. The former plot places the coordinate triads in the appropriate place in ECI, for visualization of the coordinate system with respect to the orbital motion. The latter show the trace of the coordinate axes' tips, their color changing from the initial color to yellow as time progresses.

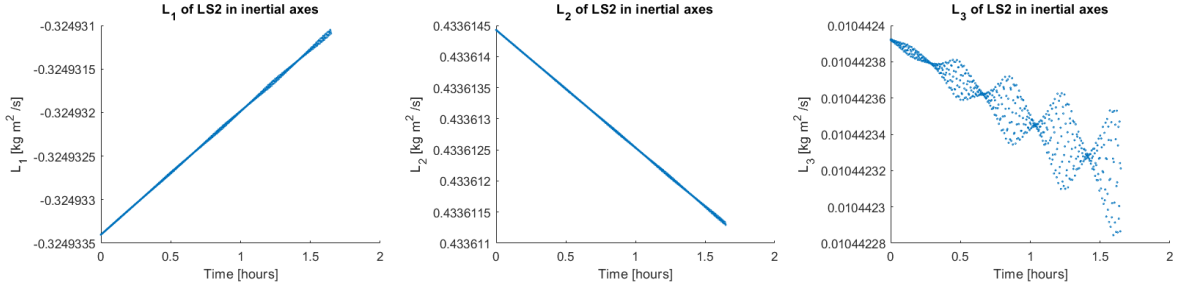


Figure 12: Components of Angular Momentum in Inertial Coordinates

4.3 EQUILIBRIUM TESTS

Placing our initial spin along the principal axis of maximum inertia and assuming that the principal axes initially correspond with the inertial axes, we can test if our attitude propagation maintains stability - we see in Fig 16 that the components of angular velocity remain constant in principal axes, as expected. Converting our quaternion output to 312 Euler angles in Fig 17, we can see that θ and ψ remain constant while ϕ increases linearly (note that the sawtooth shape comes from the angle being wrapped to 2π).

If we instead assume that our principal axes align with the RTN frame initially, with the angular velocity oriented along the N axis, our angular velocity components once again remain constant (so long as we ignore any orbital perturbations), as seen in Fig 18. This behavior initially may seem strange, as the RTN frame is non-inertial, but with spin around the principal z-axis, our angular velocity is stable; furthermore, the N axis remains constant due to the lack of orbital perturbations (no torques keep the angular momentum vector, \vec{h} , constant).

4.4 STABILITY TESTS

Once again initially aligning the principal axes with the inertial, we test the stability of spin about the three principal axes with minor perturbations. This effect is generated by providing a spin of 7 deg/s about the principal axis in question, and giving a small spin of 0.01 deg/s about the other two principal axes. The results of these stability simulations (principal-axes angular velocity, momentum, and Euler angles) are provided in Figs 19 - 21 - note that in general, the rapid switching between complementary values for Euler angles is due to the inverse trigonometric functions used in converting from quaternions to 312 Euler angles.

For an initial spin about the X-axis, the axis of least inertia, we see *periodic stability* in angular velocity and instability in angles in Fig 19.

For an initial spin about the Y-axis, the axis of intermediate inertia, we see *instability* in angular velocity and instability in angles in Fig 20.

For an initial spin about the Z-axis, the axis of maximum inertia, we see *periodic stability* with a much higher frequency in angular velocity and instability in angles in Fig 21.

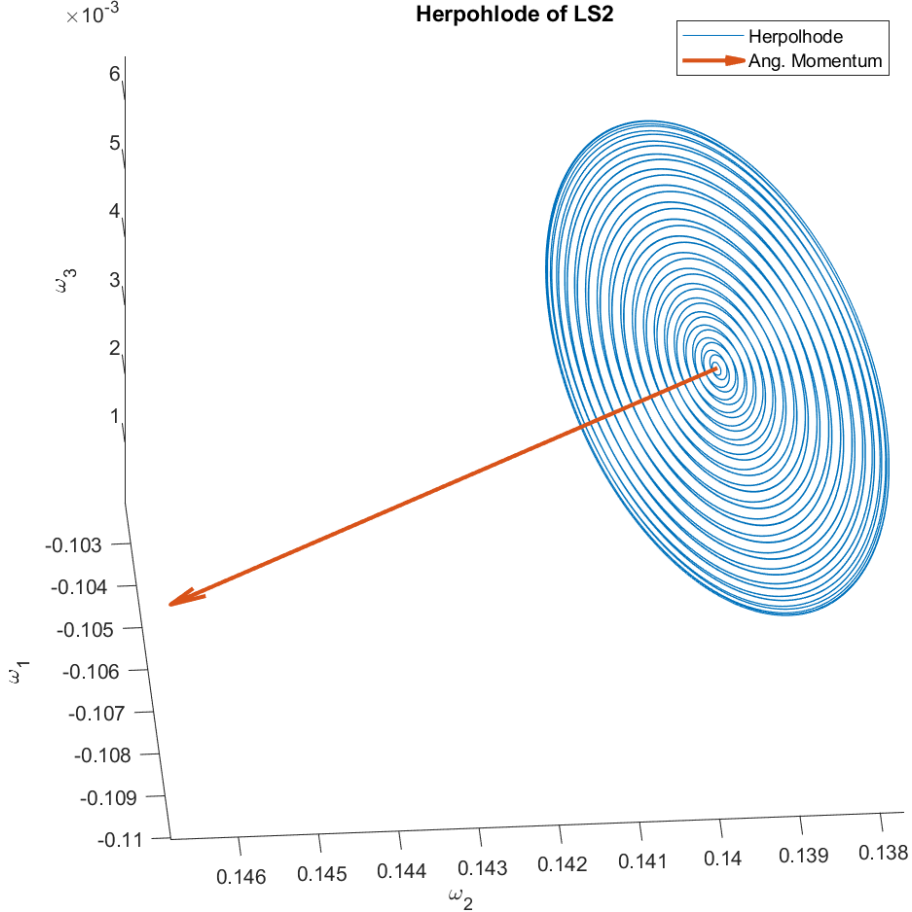


Figure 13: Herpolhode of LS2 spacecraft in plane

5 PROBLEM SET 4

5.1 DUAL SPIN

By adding a momentum wheel into our simulation (as seen in Fig 22), we give the spacecraft the capacity to perform maneuvers and ensure stability along an axis of choice. In Appendix G, we validate our new dynamics by testing the equilibrium and stability cases from the previous problem set, but now with an applied angular momentum in the momentum wheel. The data used for our momentum wheel's moment of inertia and maximum spin rate is pulled from the LS2 parts list [5], which indicates that LS2 uses a RW3-0.060 momentum wheel from Sinclair Interplanetary.

To give stability along our intermediate axis (the principal Y), we can place the rotor's axis along Y and give it a spin such that

$$I_r \omega_r > (I_z - I_y) \bar{\omega}_y$$

where I_r is the rotor's moment of inertia and $\bar{\omega}_y$ is the desired equilibrium spin rate. By setting our initial angular velocity to be equivalent to that used in our Y -axis stability test, we can cross-compare our results. In Fig 23, we can see the resulting inertial-axes angular velocity components and the 312 Euler angles that result from our simulation. Unlike in our stability test for the intermediate axis, we now see that our spin is stable with the added help of a momentum wheel along principal Y axis (note that oscillations in ω_y are very small in magnitude, and that

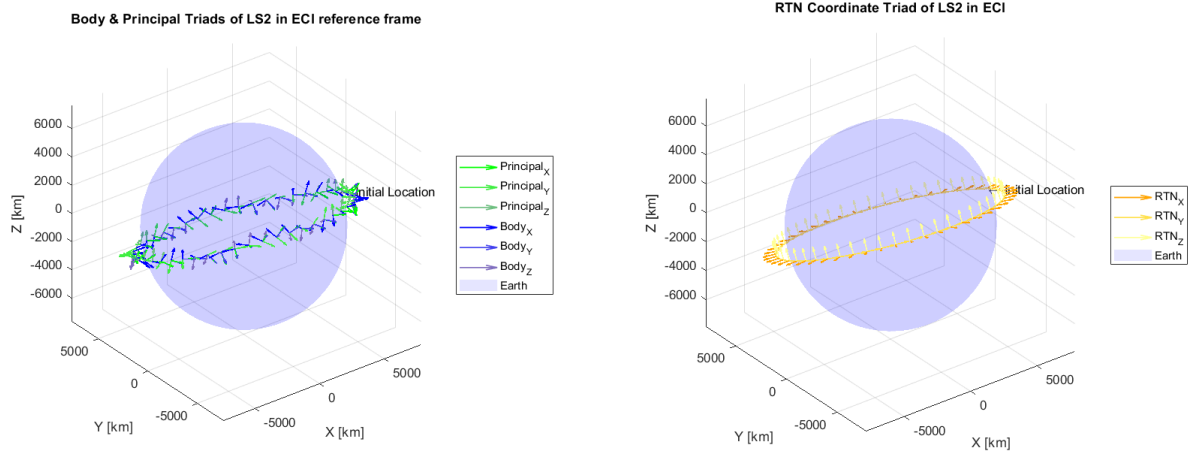


Figure 14: Coordinate triads motion in ECI

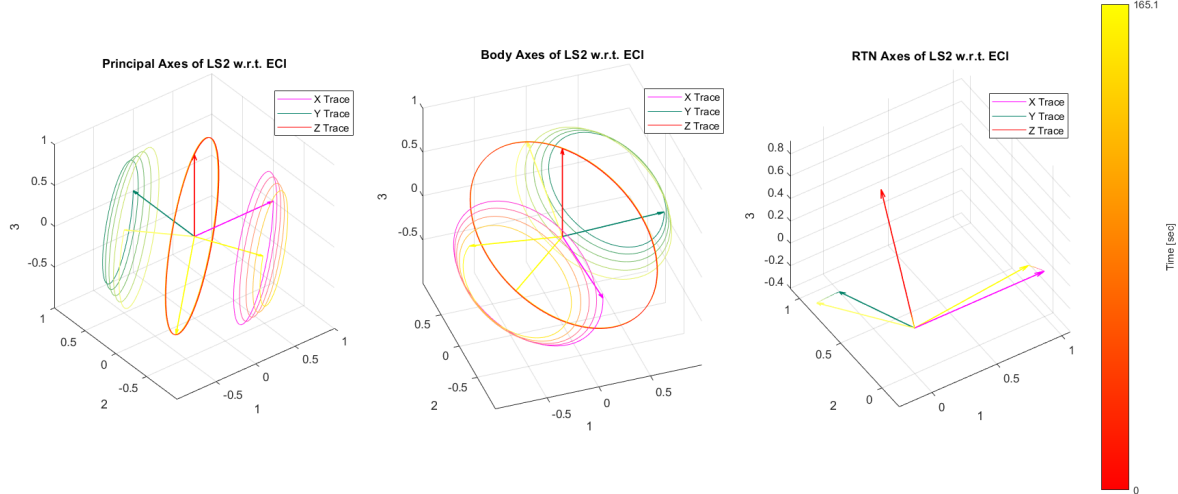


Figure 15: Coordinate triad motion in time

only ψ increases linearly while the other two Euler angles remain near 0° or 360°). This is incredibly useful given that our mission requirements require Y -axis slewing for Sun-pointing, and maintaining stable spin about this axis can help to prevent tumbling.

We can additionally attempt to ensure stability about the principal Z axis without spinning the spacecraft about the Z axis. This would be useful directly before Y axis slew maneuvers, allowing a precise understanding of how momentum wheel changes will change the inertial alignment of the Z axis. Giving the spacecraft an initial angular velocity of 0.01 deg/s about each principal axis, we put the momentum wheel axis along Z and spin it to 100 rad/s (with such a small Z spin, just about any non-trivial momentum wheel spin will suffice to ensure stability). The results of this trial can be seen in Fig 24 - note that just as in our stability test with spin primarily along the Z axis, we see periodic stability of the spacecraft angular velocity but without significant Z spin!

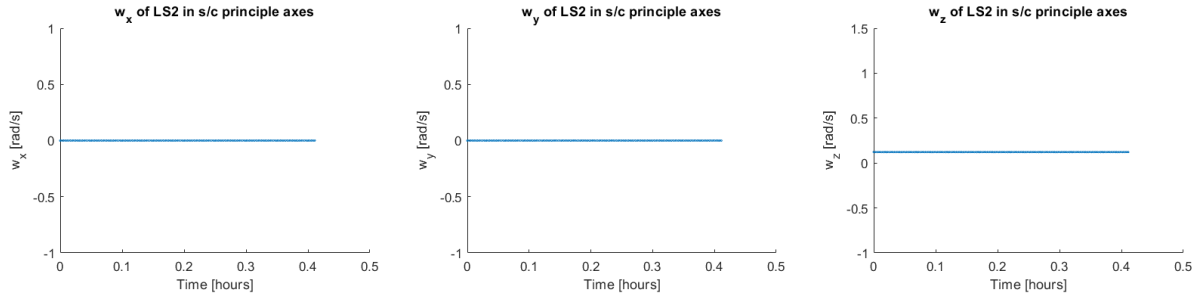


Figure 16: Components of angular velocity for spin along principal Z axis

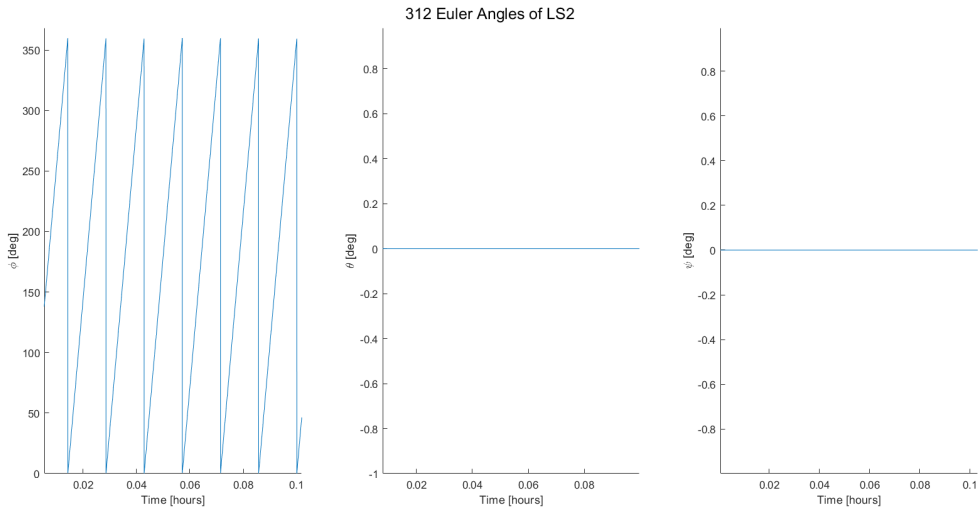


Figure 17: 312 Euler angles for spin along principal Z axis

5.2 GRAVITY GRADIENT TORQUE

The spacecraft torque due to a gravity gradient is modeled using Eq. 2 (included within the "Add environmental perturbations" block as see in Fig 22).

$$\vec{M} = \frac{3GM}{R^3} \begin{bmatrix} (I_z - I_y)c_yc_z \\ (I_x - I_z)c_zc_x \\ (I_y - I_x)c_xc_y \end{bmatrix} \quad (2)$$

Using $a_0 = 7080.6$ km in an arbitrary direction (not aligned with the RTN frame), a back-of-the-envelope calculation yields gravity gradient torques on the order of 10^{-6} in Y, Y and 10^{-9} in Z . When simulated with the same initial conditions as in Section 3.2, we see torques that match this calculation (Fig. 25).

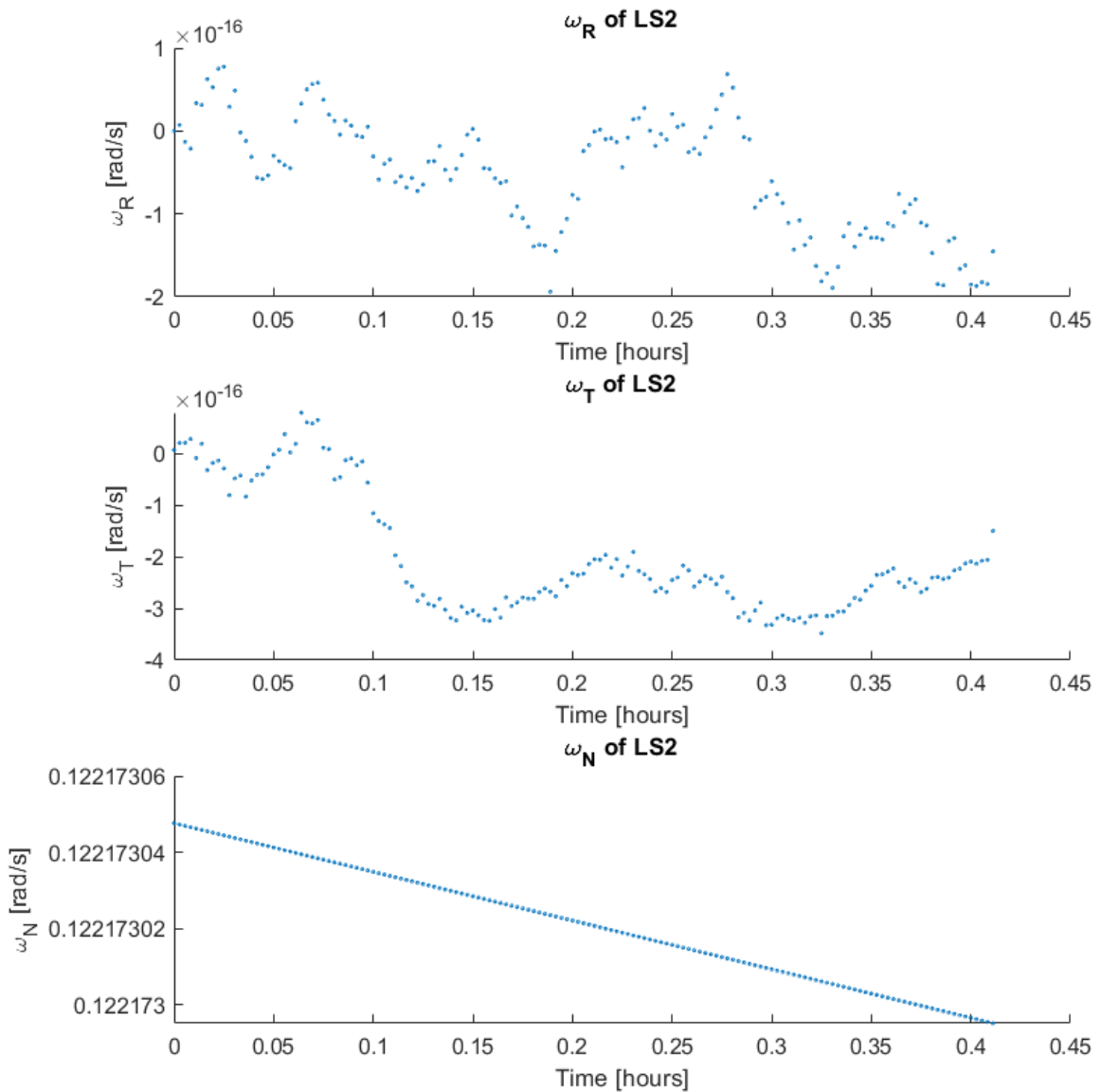


Figure 18: Components of angular velocity in RTN frame, with spin along N axis

6 REFERENCES

- [1] Chris Biddy and Tomas Svitek. “LightSail-1 Solar Sail Design and Qualification”. In: 2012.
- [2] George C. Marshall Space Flight Center. *NASA Facts: NanoSail-D*. https://www.nasa.gov/centers/marshall/pdf/484314main_NASAfactsNanoSail-D.pdf. Accessed: 4-6-2021.
- [3] Jason Davis. *What's the Difference between LightSail 1 and LightSail 2?* <https://www.planetary.org/articles/difference-between-lightsails>. Accessed: 4-6-2021. June 2019.
- [4] *Endurosat 3U Solar Panel*. <https://www.endurosat.com/cubesat-store/cubesat-solar-panels/3u-solar-panel-xy/>. Accessed: 4-3-2021.

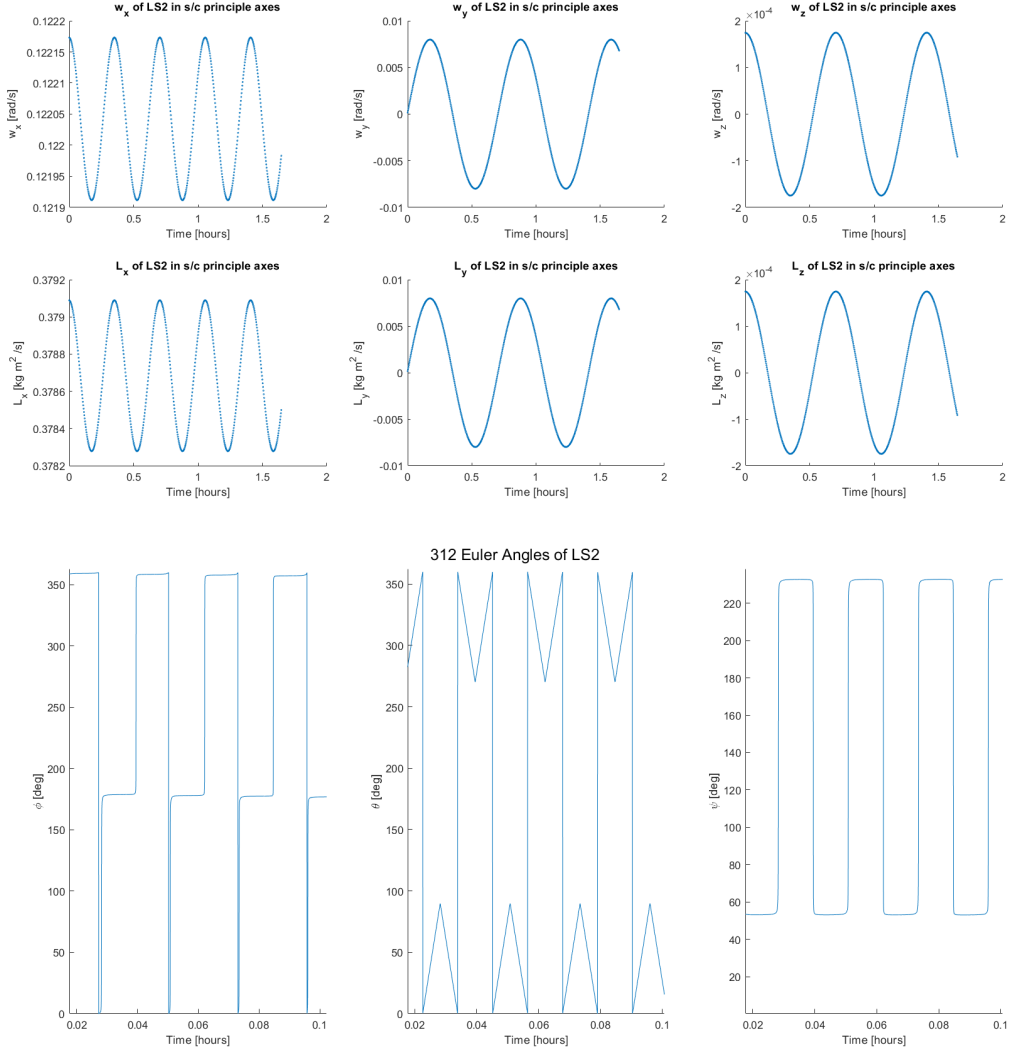


Figure 19: Velocities, angular momentum, and 312 Euler angles for principal X-axis spin.

- [5] *Lightsail 2: Parts List*. Accessed: 4-3-2021. 2017.
- [6] Barbara Plante et al. “LightSail 2 ADCS : From Simulation to Mission Readiness”. In: 2016.
- [7] Rex W. Ridenoure et al. “Testing The LightSail Program: Advancing Solar Sailing Technology Using a CubeSat Platform”. In: 2016.
- [8] The Planetary Society. *LIGHTSAIL 2 MISSION CONTROL*. https://secure.planetary.org/site/SPageNavigator/mission_control.html. Accessed: 4-6-2021.
- [9] Yuichi Tsuda et al. “Achievement of IKAROS – Japanese deep space solar sail demonstration mission”. In: *Acta Astronautica* 82.2 (2013), pp. 183–188. ISSN: 0094-5765. DOI: <https://doi.org/10.1016/j.actaastro.2012.03.032>. URL: <https://www.sciencedirect.com/science/article/pii/S0094576512001348>.

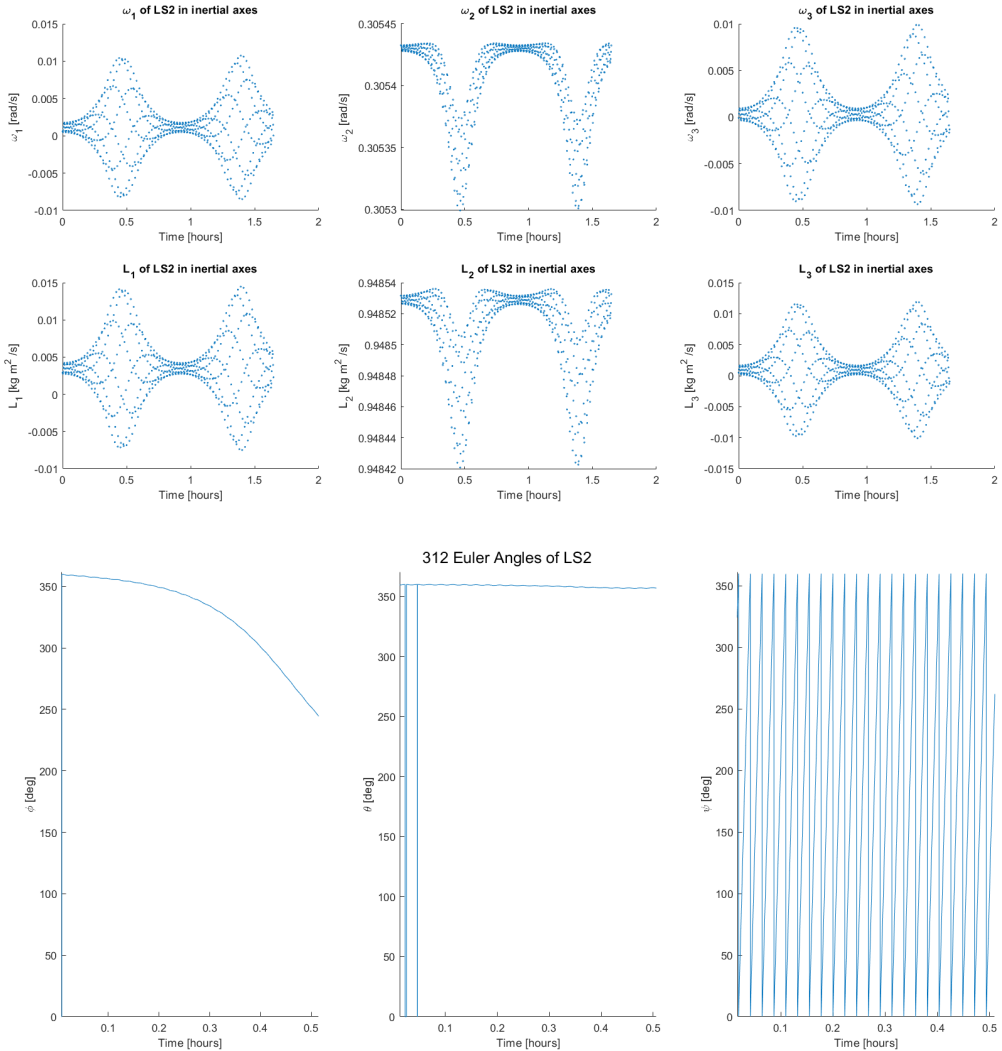


Figure 20: Velocities, angular momentum, and 312 Euler angles for principal Y-axis spin.

Appendices

A Mass Distribution Analysis

The total mass of the LS2 system is quoted as 4.93kg [7] - using various published resources from the Planetary Society and the drawings in Appendix B, we are able to make rough estimates for the masses of the five primary components: the solar sail, the sail booms, the forward body, the solar panels, and the rear body.

A.1 Solar Sail

We estimate the full mass of the solar sail system (solar sails, sail booms, boom extension mechanism, and sail housing) to be 2.9kg, based off a note from a deployment package development summary stating that the whole deployment system was contained in a package with mass " <3 kg" [1]. The sail housing, which is located in the rear body of the system, we estimate as ≈ 500 g. The solar sails, made of mylar with density $1.38 \frac{\text{g}}{\text{cm}^3}$, have a total volume of

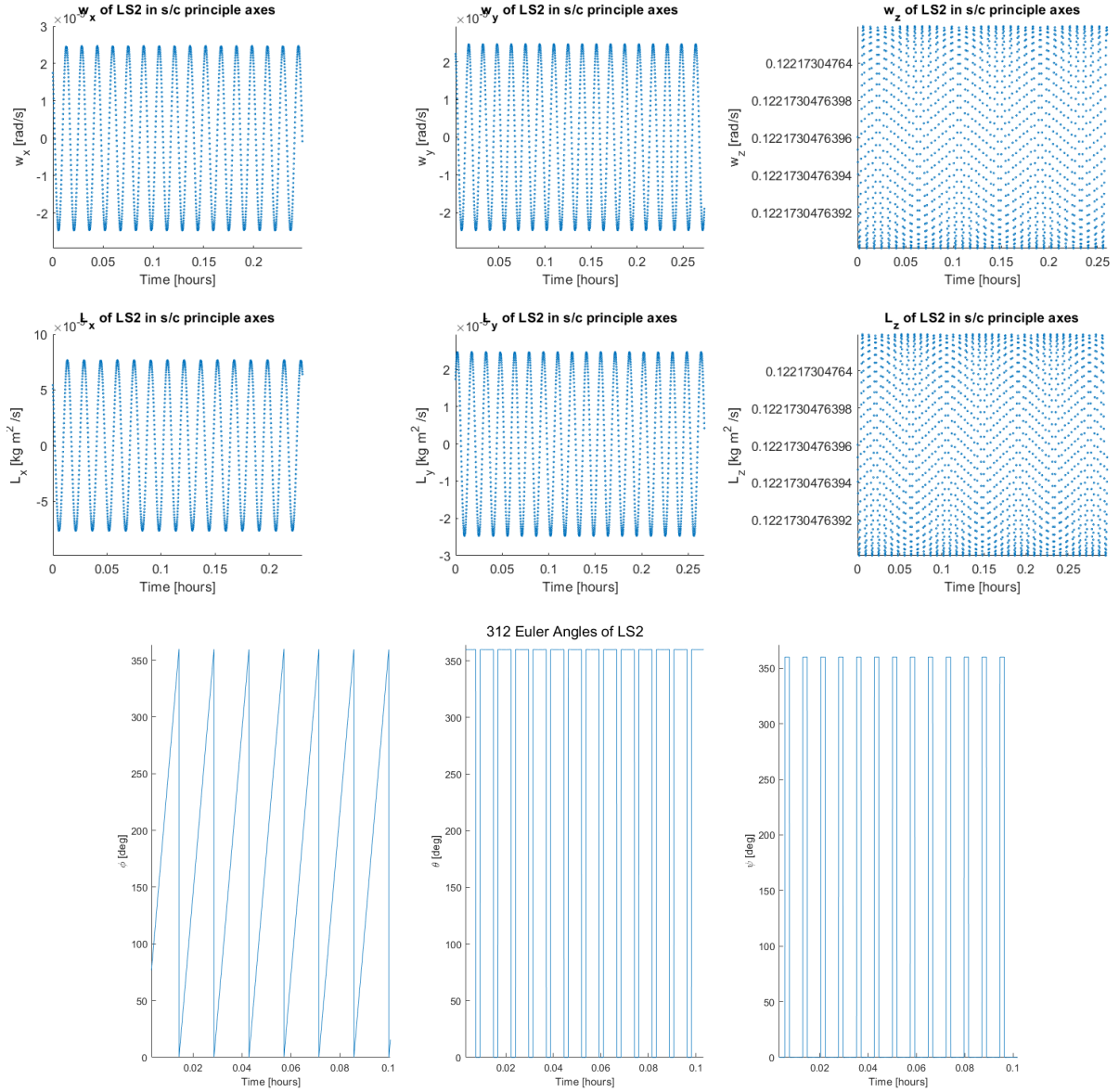


Figure 21: Velocities, angular momentum, and 312 Euler angles for principal Z-axis spin.

$5.57\text{m} \times 5.57\text{m} \times 4.5\mu\text{m}$ per the LS2 drawings. The total mass of the solar sails is therefore estimated as 0.19872 kg .

A.2 Sail Booms

The sail booms, made of elgiloy with density $8.3 \frac{\text{g}}{\text{cm}^3}$ [7], have a volume of $3.5\text{cm} \times 0.02\text{cm} \times 4\text{m}$ per the LS2 drawings. The total mass of each sail boom is therefore estimated as 0.2324 kg .

A.3 Forward Body

The forward body contains the communications avionics (transceiver board and antenna) as well as the boom extension mechanism. We can estimate the mass of the boom extension mechanism by subtracting the assumed 500g mass of the sail housing, the 198.72g of solar sail mass, and the 232.4g mass of the four sail booms from the estimated solar sail system mass

| Description | Mass, kg |
|--------------------|---------------|
| Momentum Wheel | 0.226 |
| Magnetorquers (x3) | 0.690 |
| Battery Cells (x8) | 0.128 |
| Avionics | ≈ 0.1 |
| Structures | ≈ 0.1 |
| Sail Housing | ≈ 0.5 |
| TOTAL | 1.744 |

Table 7: Estimated Mass Breakdown of Rear Body

of 2.9kg. By adding to that an estimated ≈ 200 g for communications components, we get the estimated mass of the forward body as 1.472 kg.

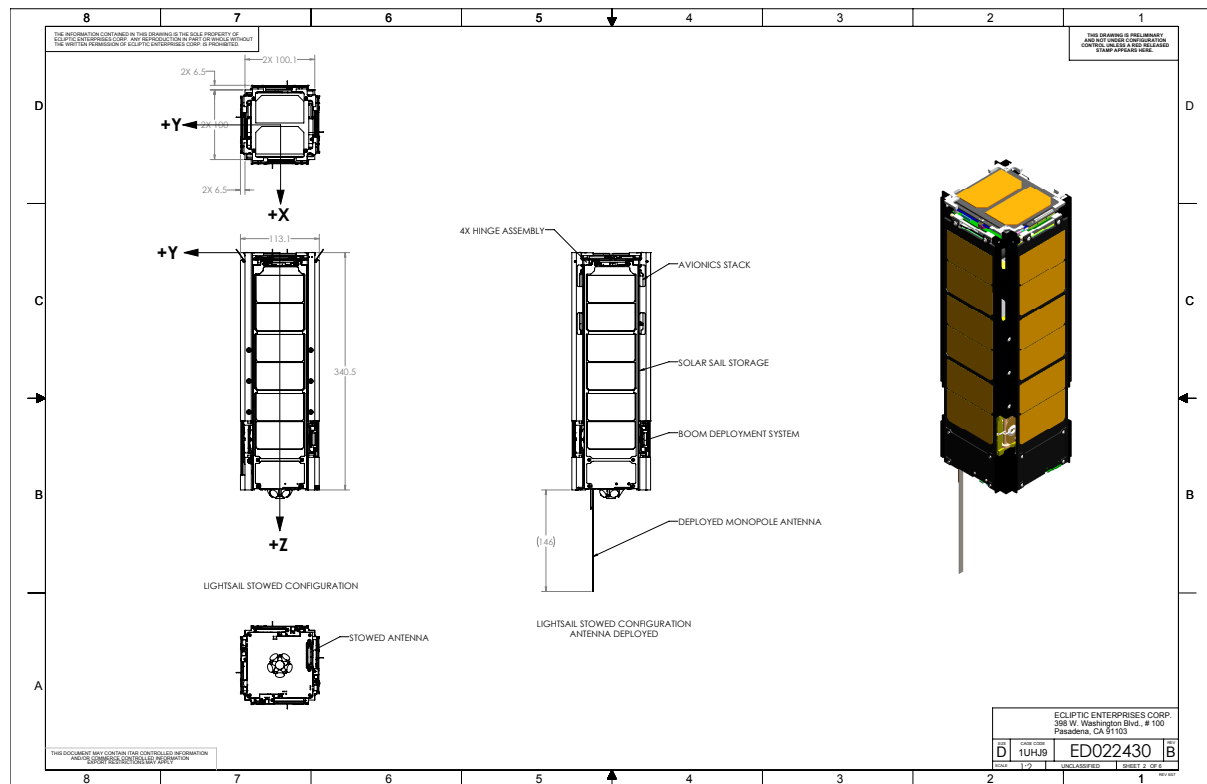
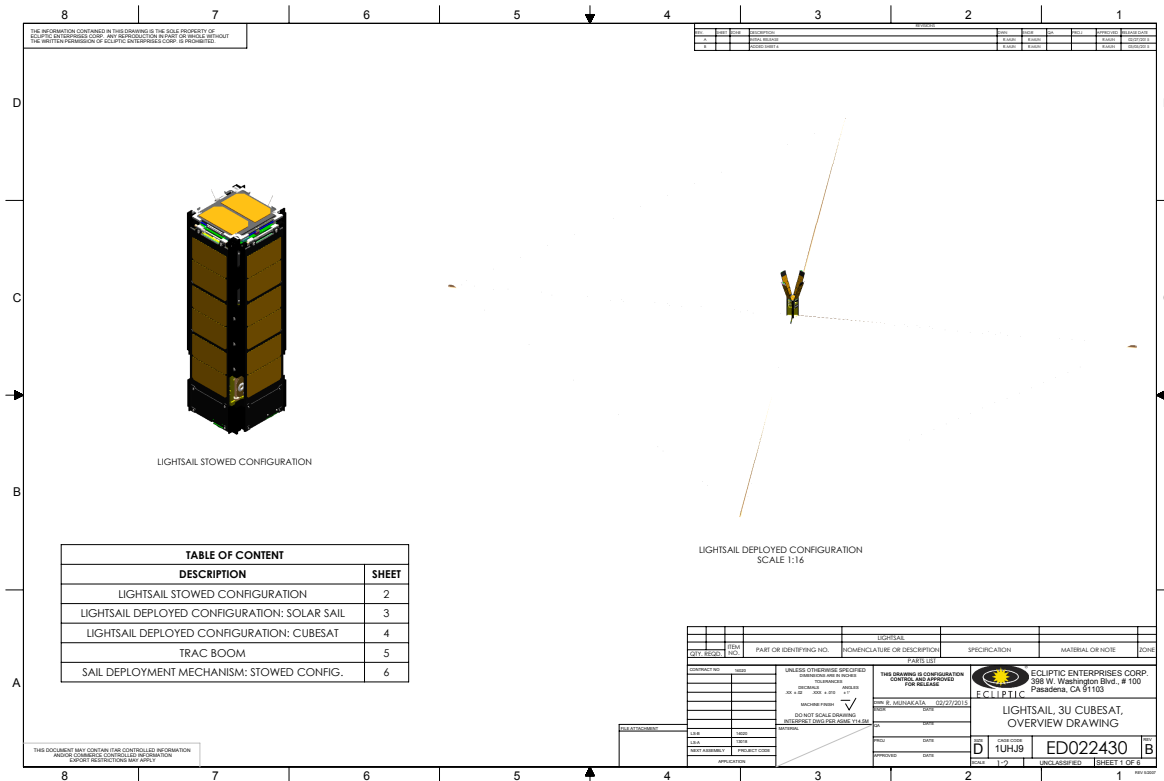
A.4 Solar Panels

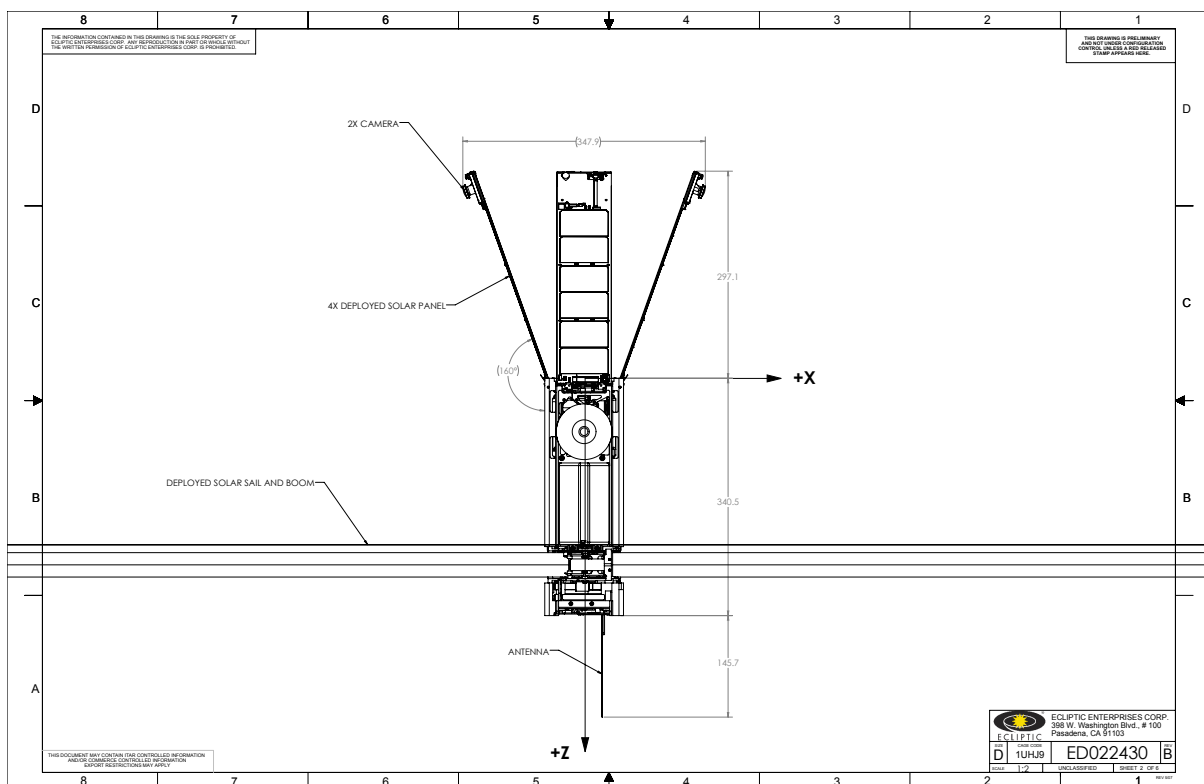
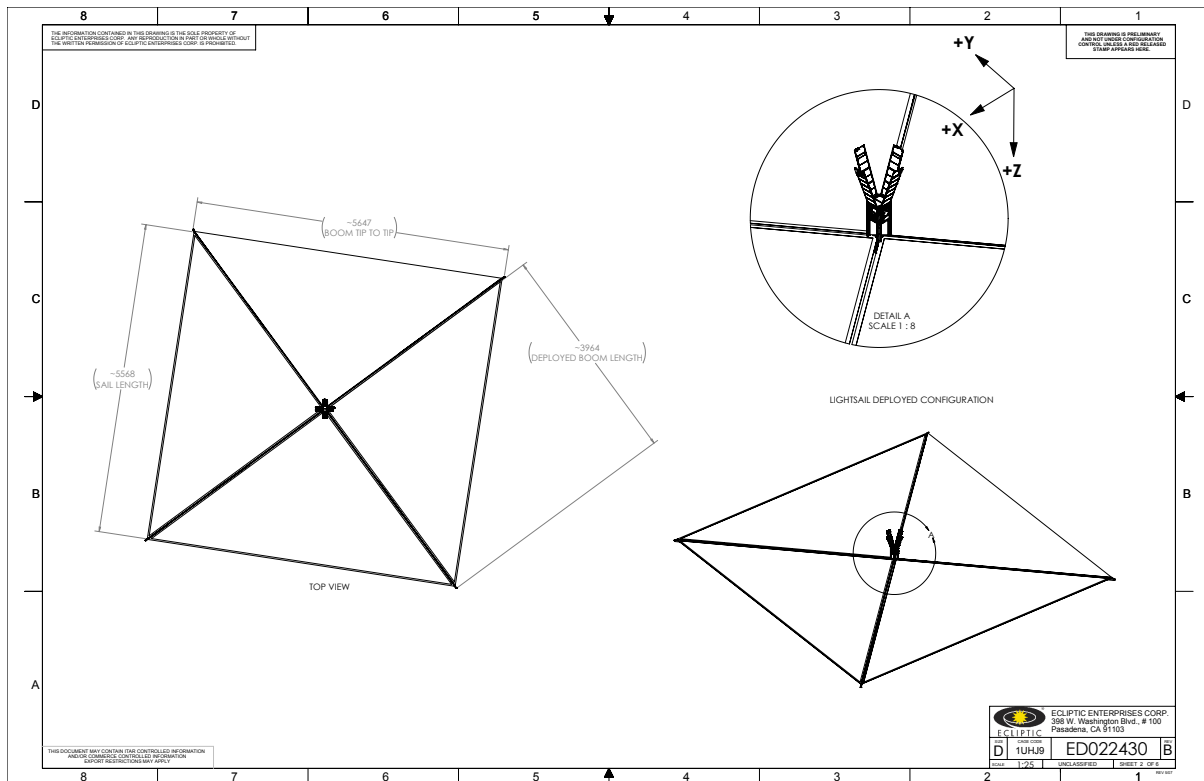
The mass of each 3U-long solar panel was estimated to be 0.150 kg based off the similar mass and form factor of Endurosat's 3U solar panel system [4].

A.5 Rear Body

The mass of the rear body was calculated implicitly by subtracting the calculated masses of the above systems from the total satellite mass. This gives an estimated rear body mass of 1.73 kg. We give some validity to this estimate by noting that the breakdown in Table 7 provides reasonable estimates for rear body component masses that total to 1.74 kg. Note that the table lists some approximate values (indicated with \approx) and some values taken from the links on the Lightsail 2 parts list [5] where available .

B LS2 System Drawings





C VBA Solidworks Macro for Exporting Surface Normals

The Solidworks VBA macro below uses a sketch to generate information about the outer geometry of a shape - the starting location of a line is taken to be the barycenter of the surface, and the unit direction is taken from the vector from the start point to the end point (normalized

by length). The area of the associated surface (in m²) is encoded in the length of the line (in m) - this is particularly easy to do in Solidworks with parameterized dimensions, and makes updating the centroids and normals an easy process, even for complicated shapes.

```

1 Dim swApp As Object
2 Sub main()
3 Dim swApp As SldWorks.SldWorks
4 Dim doc As SldWorks.ModelDoc2
5 Dim assembly As SldWorks.AssemblyDoc
6 Dim sm As SldWorks.SelectionMgr
7 Dim eq As SldWorks.EquationMgr
8 Dim feat As SldWorks.Feature
9 Dim sketch As SldWorks.sketch
10 Dim v As Variant
11 Dim i As Long
12 Dim sseg As SldWorks.SketchSegment
13 Dim sline As SldWorks.SketchLine
14 Dim sp As SldWorks.SketchPoint
15 Dim ep As SldWorks.SketchPoint
16 Dim s As String
17 Dim CMx, CMy, CMz As Double
18
19
20
21 Set exApp = CreateObject("Excel.Application")
22 If Not exApp Is Nothing Then
23   exApp.Visible = True
24   If Not exApp Is Nothing Then
25     exApp.Workbooks.Add
26     Set sheet = exApp.ActiveSheet
27     If Not sheet Is Nothing Then
28       sheet.Cells(1, 1).Value = "X (m)"
29       sheet.Cells(1, 2).Value = "Y (m)"
30       sheet.Cells(1, 3).Value = "Z (m)"
31       sheet.Cells(1, 4).Value = "Normal X"
32       sheet.Cells(1, 5).Value = "Normal Y"
33       sheet.Cells(1, 6).Value = "Normal Z"
34       sheet.Cells(1, 7).Value = "Area (m*m)"
35     End If
36   End If
37 End If
38
39
40 Set swApp = GetObject(, "sldworks.application")
41 If Not swApp Is Nothing Then
42   Set doc = swApp.ActiveDoc
43   If Not doc Is Nothing Then
44     If doc.GetType = swDocASSEMBLY Then
45       Set assembly = doc
46       Set sm = doc.SelectionManager
47       Set eq = doc.GetEquationMgr
48       If Not assembly Is Nothing And Not sm Is Nothing Then
49         Dim j, m As Long
50         m = eq.GetCount
51         For j = 0 To m - 1
52           If InStr(1, eq.Equation(j), "SW-CenterofMassX") Then
53             CMx = eq.Value(j)

```

```

54         ElseIf InStr(1, eq.Equation(j), "SW-CenterofMassY") Then
55             CMy = eq.Value(j)
56         ElseIf InStr(1, eq.Equation(j), "SW-CenterofMassZ") Then
57             CMz = eq.Value(j)
58         End If
59     Next j
60
61     If sm.GetSelectedObjectType2(1) = swSelSKETCHES Then
62         Set feat = sm.GetSelectedObject6(1, -1)
63         Set sketch = feat.GetSpecificFeature2
64         If Not sketch Is Nothing Then
65             v = sketch.GetLines2(1)
66             numlines = sketch.GetLineCount2(1)
67             Dim c As Long
68             c = 0
69             For i = 0 To numlines - 1
70                 If Not sheet Is Nothing And Not exApp Is Nothing Then
71
72                     Dim myType As Double
73                     myType = (v(12 * i + 2))
74
75                     If myType < 1 Then
76
77                         Dim startX, startY, startZ, endX, endY, endZ, myL As Double
78                         startX = (v(12 * i + 6))
79                         startY = (v(12 * i + 7))
80                         startZ = (v(12 * i + 8))
81                         endX = (v(12 * i + 9))
82                         endY = (v(12 * i + 10))
83                         endZ = (v(12 * i + 11))
84                         myL = Sqr(((startX - endX) ^ 2) + ((startY - endY) ^ 2) ...
85                                     + ((startZ - endZ) ^ 2))
86                         sheet.Cells(2 + c, 1).Value = startX - CMx
87                         sheet.Cells(2 + c, 2).Value = startY - CMy
88                         sheet.Cells(2 + c, 3).Value = startZ - CMz
89                         sheet.Cells(2 + c, 4).Value = (endX - startX) / myL
90                         sheet.Cells(2 + c, 5).Value = (endY - startY) / myL
91                         sheet.Cells(2 + c, 6).Value = (endZ - startZ) / myL
92                         sheet.Cells(2 + c, 7).Value = myL
93                         exApp.Columns.AutoFit
94                         c = c + 1
95                     End If
96                 Next i
97             End If
98         End If
99     End If
100    End If
101   End If
102 End If
103 End Sub

```

D Verification of Inertia Computations

For our analytical calculations, we will ignore asymmetric components, and place the associated mass of each primary component at its geometric centroid (this is a fairly safe assumption,

given the layout of our satellite). This will greatly simplify our calculations.

We begin with two basic equations; first, the moments of inertia of a rectangular prism with length a along its principal x axis, length b along its principal y axis, length c along its principal z axis, and mass m :

$$\begin{aligned} I_{xx} &= \frac{1}{12}m(b^2 + c^2) \\ I_{yy} &= \frac{1}{12}m(a^2 + c^2) \\ I_{zz} &= \frac{1}{12}m(a^2 + b^2) \end{aligned}$$

We will also need the formula for a rectangular prism tilted about an axis, as the sail booms are at a 45° angle w.r.t the z axis and the solar panels are tilted at 20° w.r.t to the x/y axes. For the sail booms, I_{zz} is the same as above, but our formula for I_{yy} will need to be modified to account for this rotation. I_{yy} for this rectangular prism (assuming the tilt angle is $\beta = 45^\circ$) is

$$I_{yy} = \frac{1}{12}m(acos\beta + bsin\beta + c)$$

For the solar panels, we will also need to use (depending on the orientation of the panel)

$$\begin{aligned} I_{zz} &= \frac{1}{12}m(acos\beta + b + csin\beta) \\ &\quad \text{if tilted w.r.t to } x \text{ or} \\ I_{zz} &= \frac{1}{12}m(a + bcos\beta + csin\beta) \\ &\quad \text{if tilted w.r.t to } y. \end{aligned}$$

We also will make use of the parallel axis theorem, which states that the moment of inertia of a body about an axis B parallel to an axis, A , can be written as

$$I_B = I_A + mr^2$$

where m is the mass of the body and r is the distance between the parallel axes.

We also recognize that due to our simplified x - y symmetry, $I_{xx} = I_{yy}$ for our purposes, and by definition, our x and y axes are aligned with the principal axes. Furthermore, due to the alignment of our body axes along the line of symmetry, we know that our full inertia matrix w.r.t the body axes is roughly

$$L = \begin{bmatrix} I_{xx} & 0 & 0 \\ 0 & I_{yy} & 0 \\ 0 & 0 & I_{zz} \end{bmatrix} = \begin{bmatrix} I_{xx} & 0 & 0 \\ 0 & I_{xx} & 0 \\ 0 & 0 & I_{zz} \end{bmatrix}$$

In Table 8, we tabulate the mass, a , b , c , and the distance between the principal axis and y/z body axes for each component (measured using the CAD model). Applying our equation for moment of inertia and parallel axis theorem, we are able to calculate the contribution of each item to I_{xx} and I_{zz} . Our final results are $I_{xx} = I_{yy} = 3.125 \text{ kg} \cdot \text{m}^2$ and $I_{zz} = 5.983 \text{ kg} \cdot \text{m}^2$, which have relative errors compared to the CAD-computed values of 0.7% and 0.02%, respectively.

Given these negligibly small errors (likely caused due to the fact that the distances between the parallel axes were measured assuming that the solar panels and booms were planes, rather than

| Component | Mass, kg | Width a, m | Length b, m | Height c, m | // to Y-Axis, m | // to Z-Axis, m | Quantity | Iyy, kg m^2 | Izz, kg m^2 |
|--------------------|-------------|------------|-------------|-------------|-----------------|-----------------|----------|--------------------|--------------------|
| Forward Body | 1.47168 | 0.1 | 0.1 | 0.11 | 0.12055 | 0 | 1 | 0.0241 | 0.0024528 |
| Sail Booms | 0.2324 | 2.00E-04 | 4 | 0.035 | 1.3249 | 1.9957 | 4 | 6.27E-01 | 1.24E+00 |
| Sail | 0.19872 | 5.57 | 5.57 | 4.50E-06 | 0.06555 | 0 | 1 | 5.15E-01 | 1.0275 |
| Rear Body | 1.73 | 0.1 | 0.1 | 0.23 | 0.04945 | 0 | 1 | 0.01330 | 0.002883 |
| Solar Panel X-Tilt | 0.15 | 6.50E-03 | 0.1 | 0.316 | 0.31294 | 0.1040 | 2 | 1.52E-02 | 2.18E-03 |
| Solar Panel Y-Tilt | 0.15 | 0.1 | 6.50E-03 | 0.316 | 0.3298 | 0.1040 | 2 | 1.76E-02 | 2.18E-03 |
| TOTAL | 4.93 | - | - | - | - | - | - | 3.125909335 | 5.983479674 |

Table 8: Tabulated Inertia Calculation Data.

prisms with finite thickness, in addition to our simplifying assumptions about mass distribution), it is clear that the CAD-computed values for the inertia characteristics of our system are trustworthy. The off-diagonal components calculate by the 3D model are trusted, as they are very close to zero.

E Additional Orbital Propagator Notes

Plots of evolution of the orbital elements used to generate Figure 4. Atmospheric drag contributes to the decrease in semimajor axis, while J2 contributes to the change in RAAN and argument of periapsis. The perturbation calculations make use of the $e \approx 0$ approximation, which is fine given the initial $e \approx 0.001$, but will need to be modified to increase fidelity as the spacecraft orbit elongates due to SRP.

F Quaternion and 312 Euler Kinematic Comparison

To validate our attitude propagation system, we compare the propagation of identical initial configurations for both quaternion kinematics and 312 Euler angle kinematics. In the series of figures below, we see the attitude propagation for both kinematics based on spin initially about the principal Y-axis (a principal axis was chosen to avoid the singularity of the 312 Euler sequence at $\Theta = \frac{\pi}{2}$). Note that all plots appear nearly exactly identical, validating the quaternion propagation method.

Furthermore, Fig 31 and 32 show the direct comparisons of the quaternion and 312 Euler output (each being converted to the other attitude for comparison, along with the raw difference error for comparison). Note that the 312 Euler strays from expected behavior the most, but error stay reasonable between the two parameterizations (note that a difference of 360 degrees is equivalent to a difference of zero).z

G Dual Spin Equilibrium & Stability Analysis

To ensure that our addition of a momentum wheel has not modified our simulation dynamics, we repeat the stability and equilibrium analyses required for Problem Set 3, but now with a spinning momentum wheel.

We test equilibrium in 4 cases - setting the momentum wheel's axis to be along a principal axis, we spin the system about the same principal axis and turn the momentum wheel on at 1 rad/s. Fig 33-34 show the resulting inertial-axes angular velocity and the associated 312 Euler angles. In the fourth case, we set the principal axes to be initially aligned with the RTN frame, then spin initially about the N axis. The resulting RTN frame angular velocity and 312 Euler angles are shown in 36. Note that as expected, our angular velocities remain constant and one Euler

angle increases linearly.

We test stability in 3 cases - setting the momentum wheel's axis to be along a principal axis, we spin the system primarily about the same axis at 7 deg/s with the momentum wheel spinning at 1 rad/s, and give minor 0.01 deg/s perturbative spins about the other two principal axes. Fig 37-38 show the resulting inertial-axes angular velocity and the associated 312 Euler angles. Note that as expected, spinning about X and Z result in periodically stable spin, while initially spinning about Y with perturbation resulting in instability.

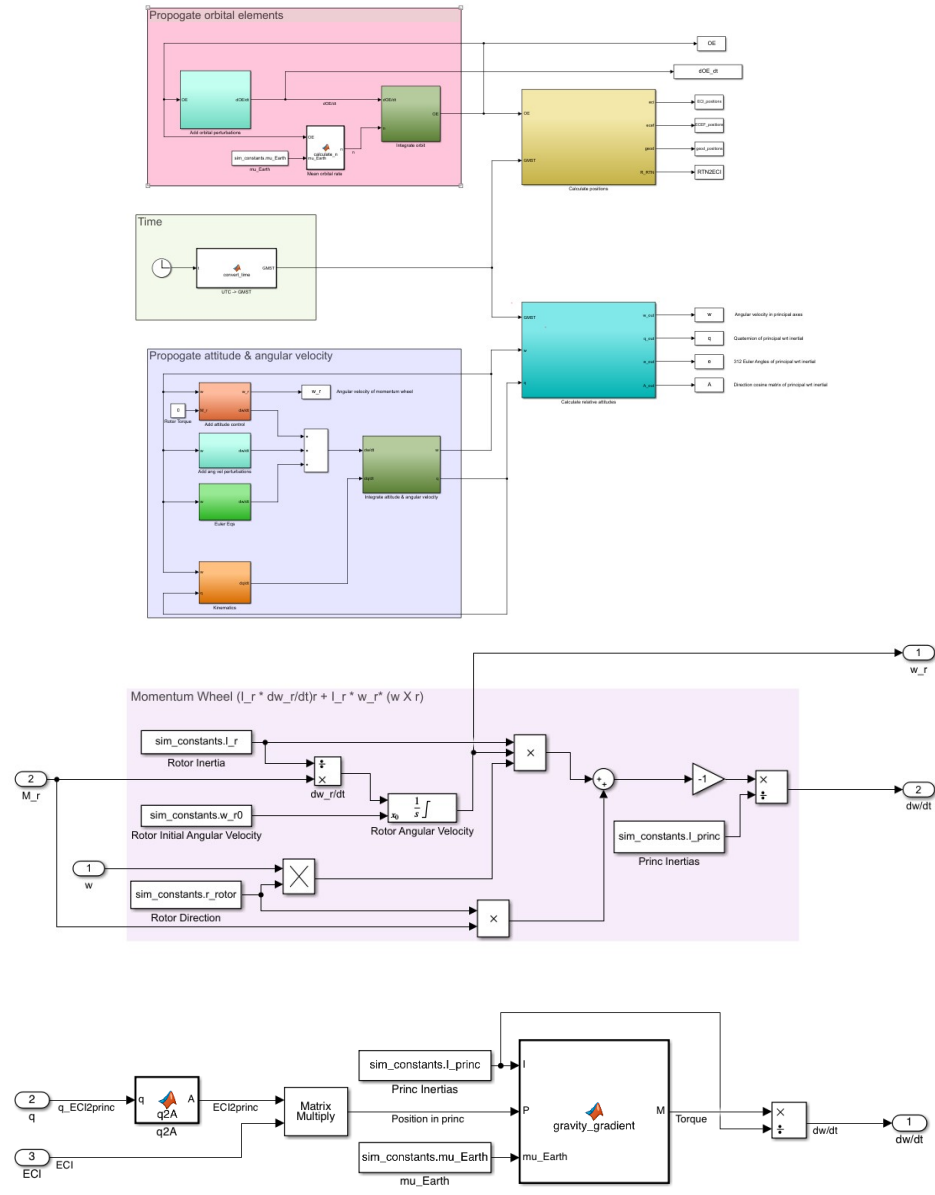


Figure 22: Updated Overview of Simulink Propagator with Momentum Wheel and Gravity Gradient Details

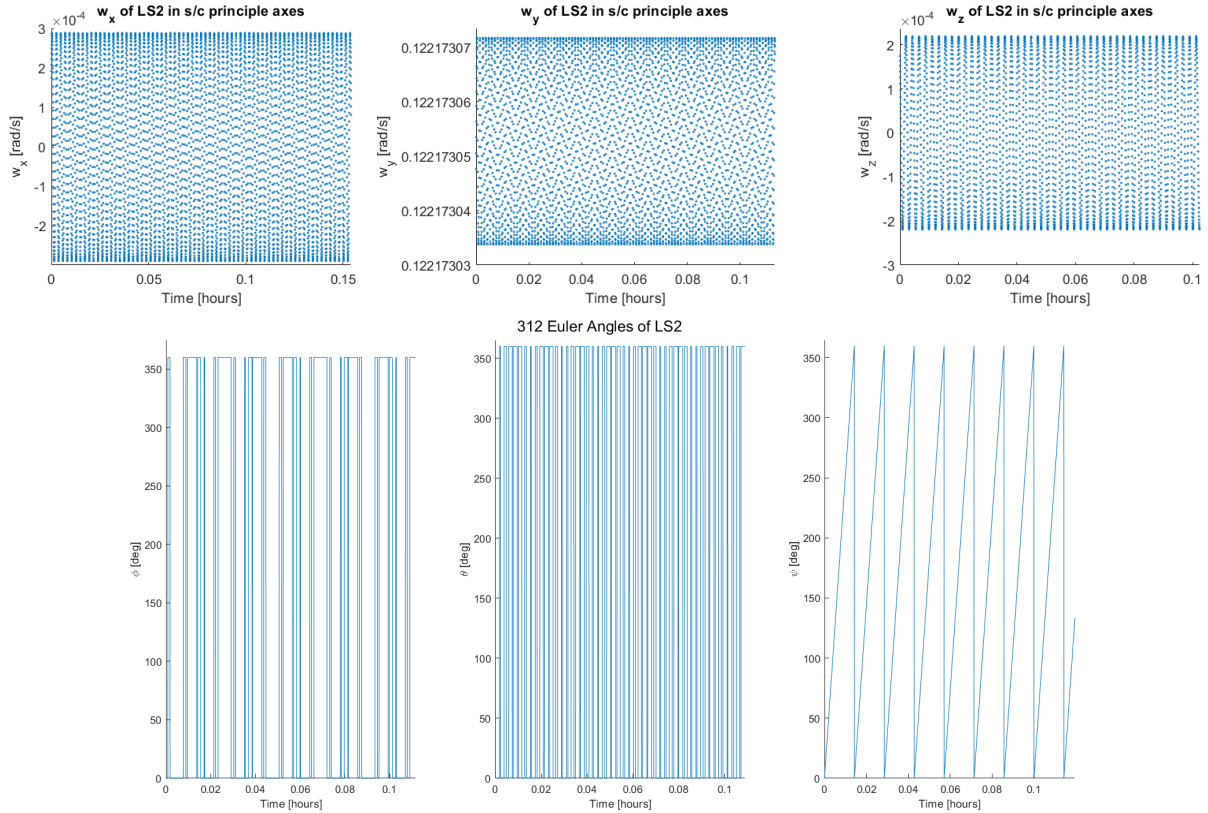


Figure 23: Angular velocity components and 312 Euler angles for intermediate axis spin, with momentum wheel for stability.

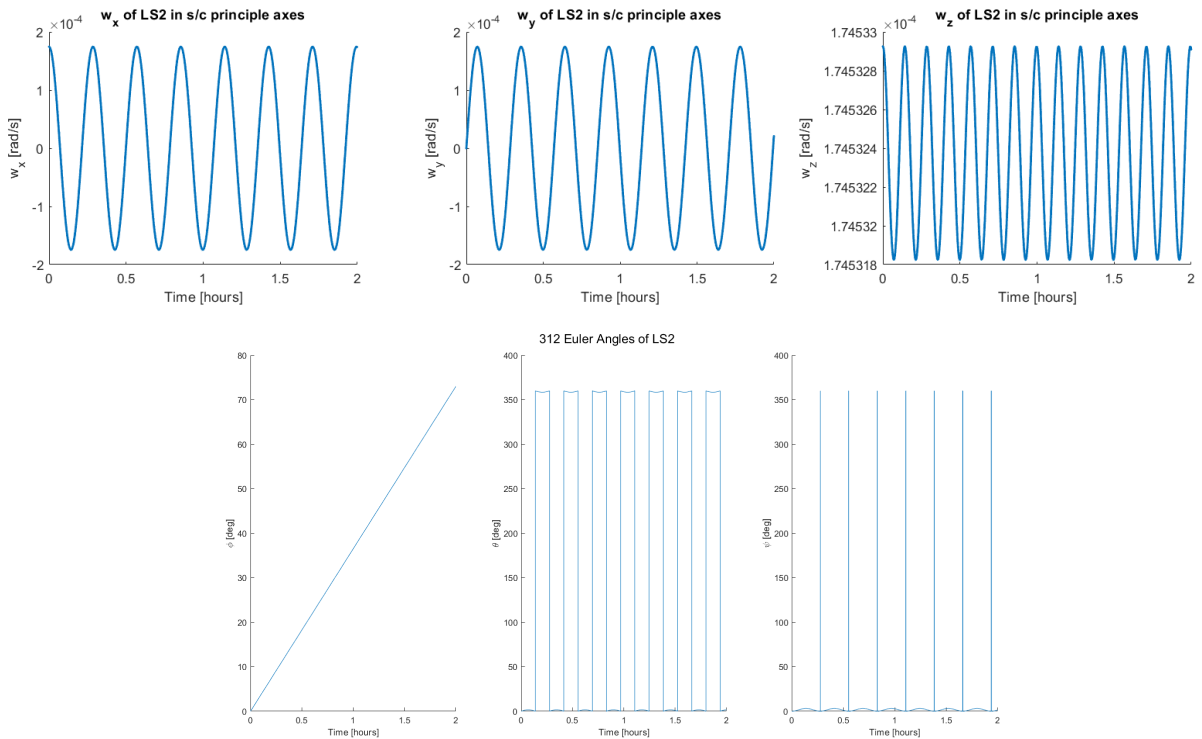


Figure 24: Angular velocity components and 312 Euler angles for low spin, with momentum wheel for Z stability.

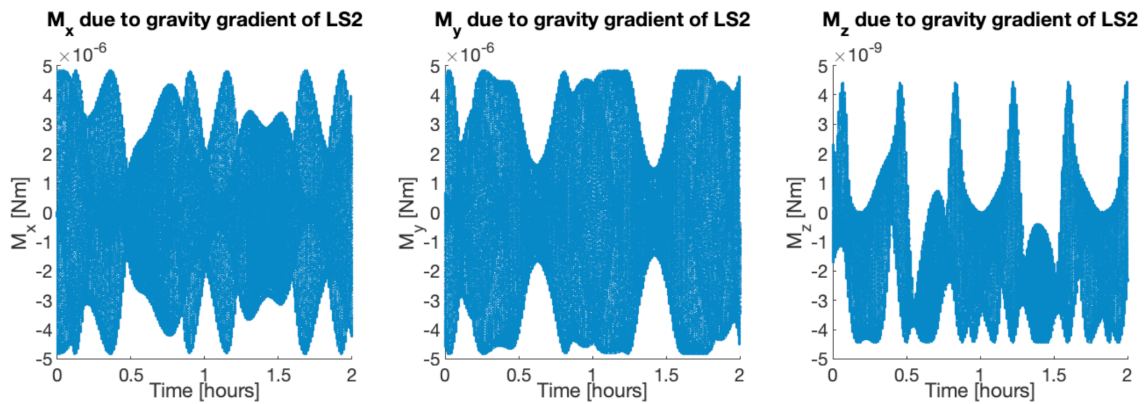


Figure 25: Torques on spacecraft principal axes due to gravity gradient.

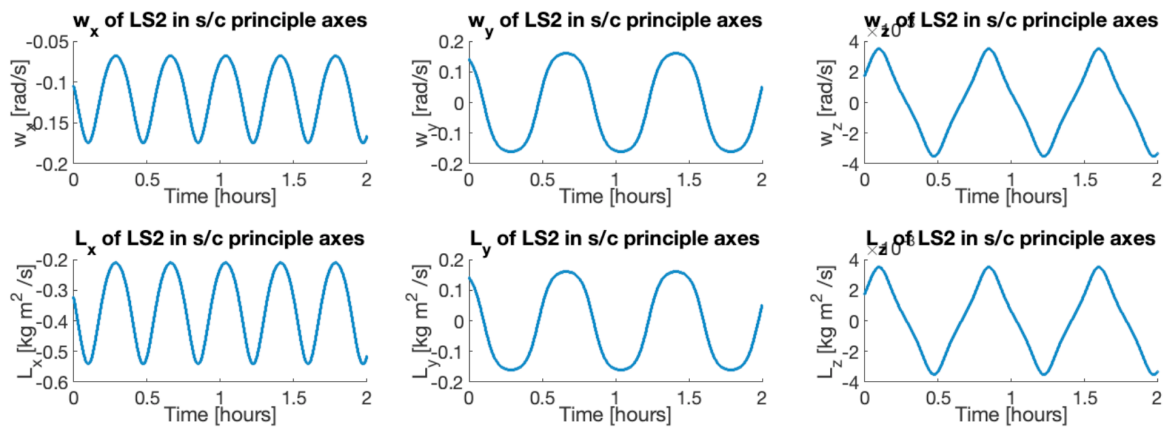


Figure 26: Angular velocity, momentum spacecraft principal axes due to gravity gradient.

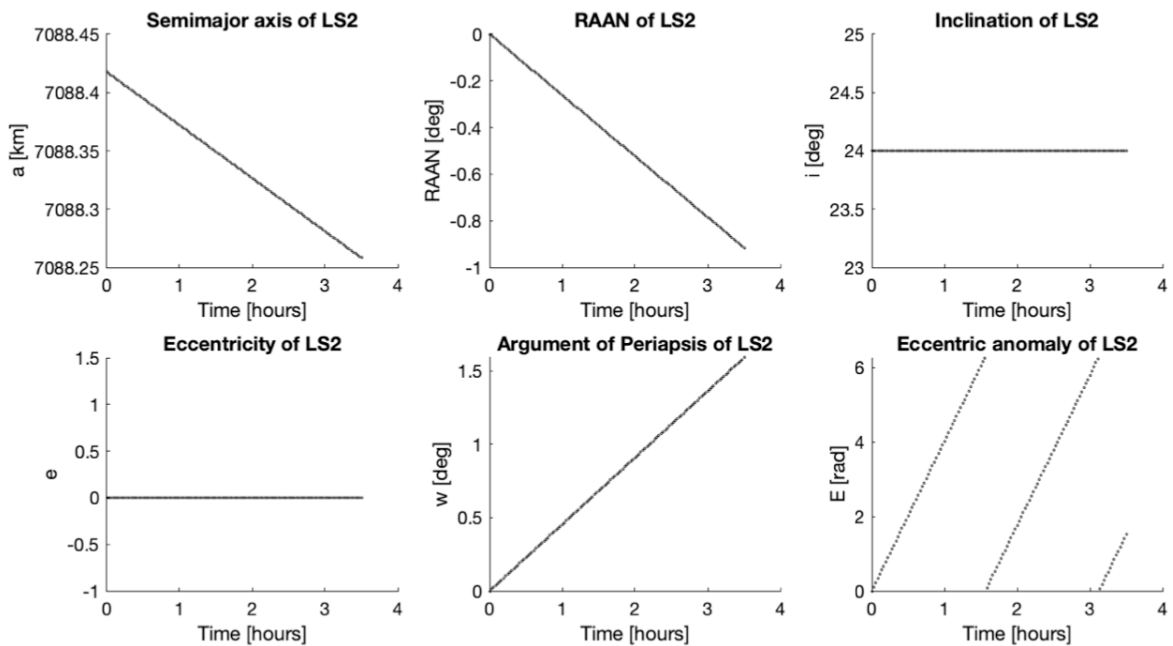


Figure 27: Keplerian orbital elements

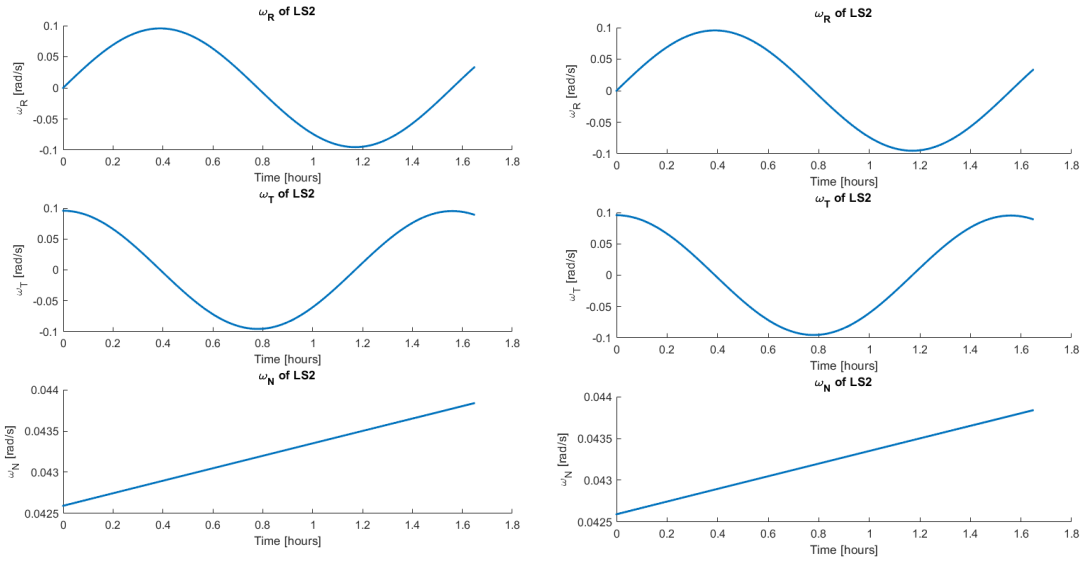


Figure 28: Angular vel. in RTN frame for Quaternion (left) and Euler 312 (right) propagation.

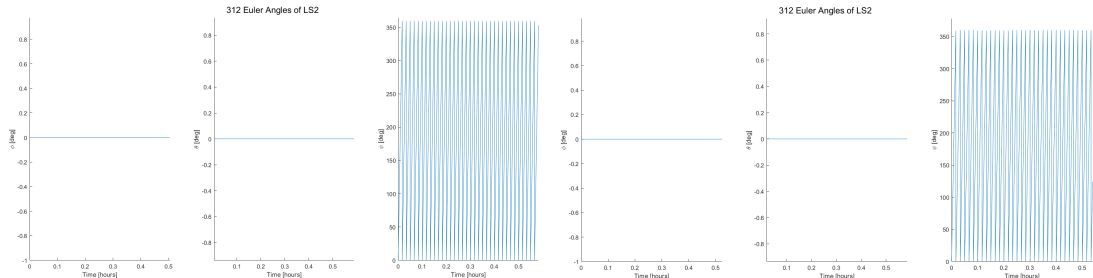


Figure 29: 312 Euler Angles for Quaternion (left) and Euler 312 (right) propagation.

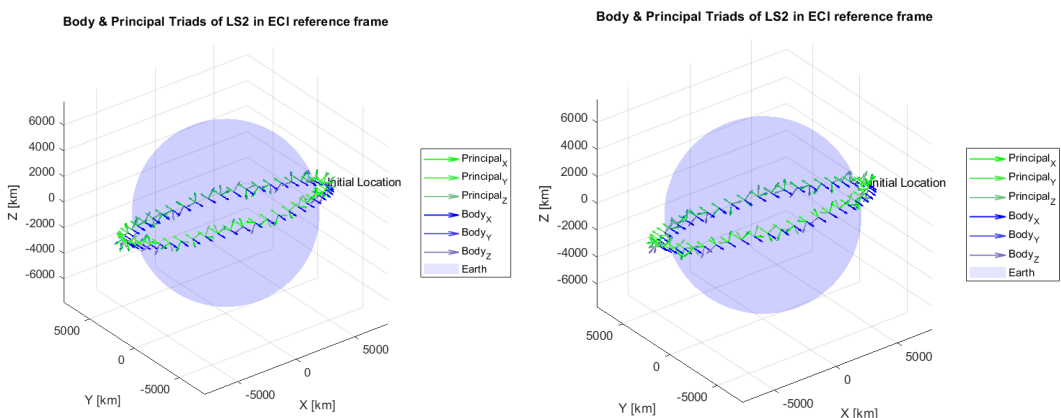


Figure 30: Coordinate triads in ECI frame for Quaternion (left) and Euler 312 (right) propagation.

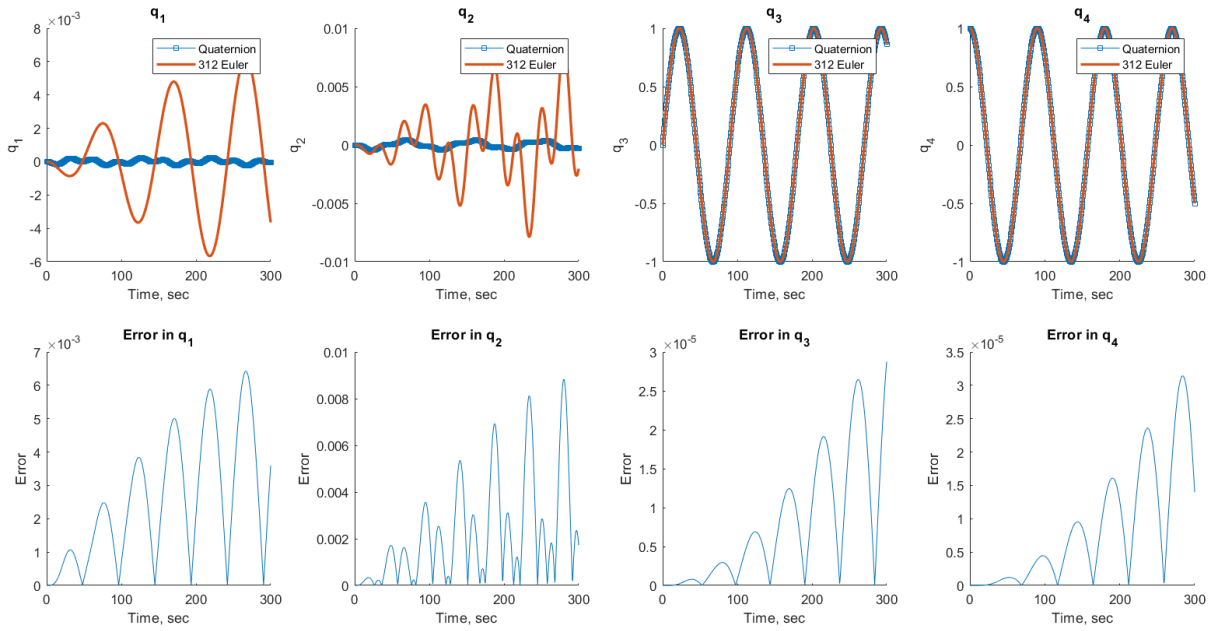


Figure 31: Comparison of quaternions from both attitude parameterizations.

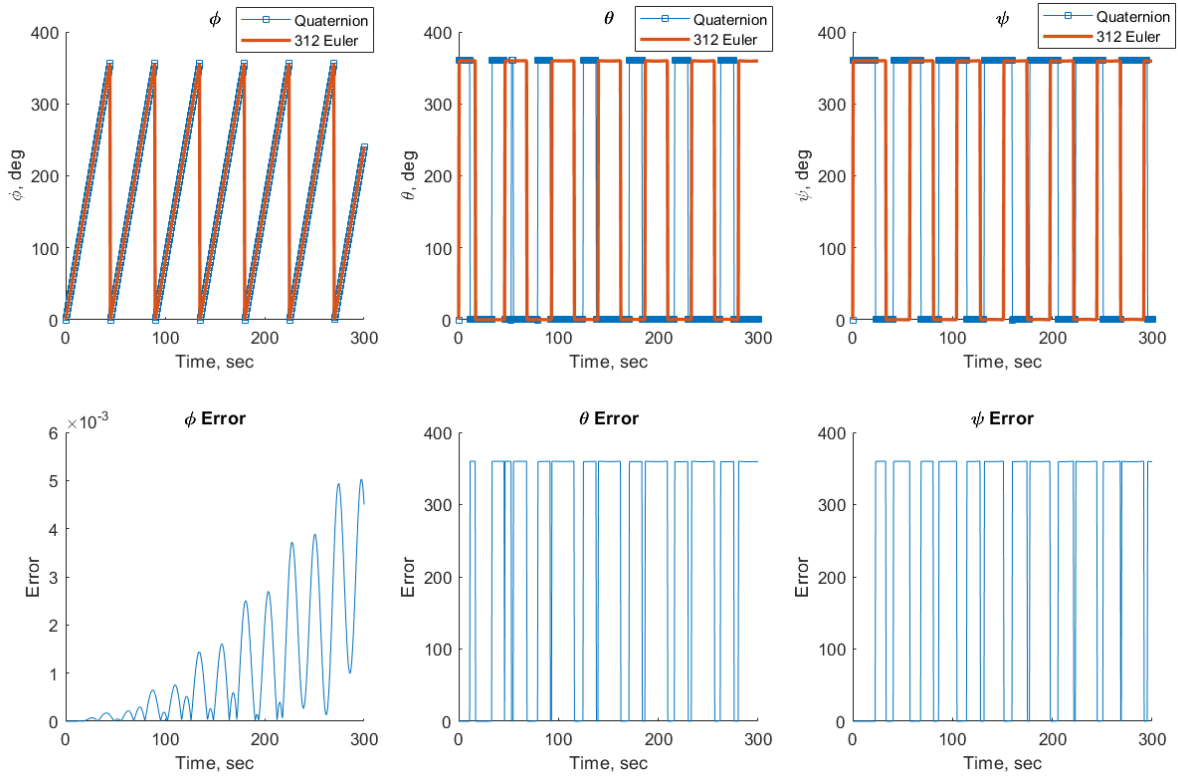


Figure 32: Comparison of Euler angles from both attitude parameterizations.

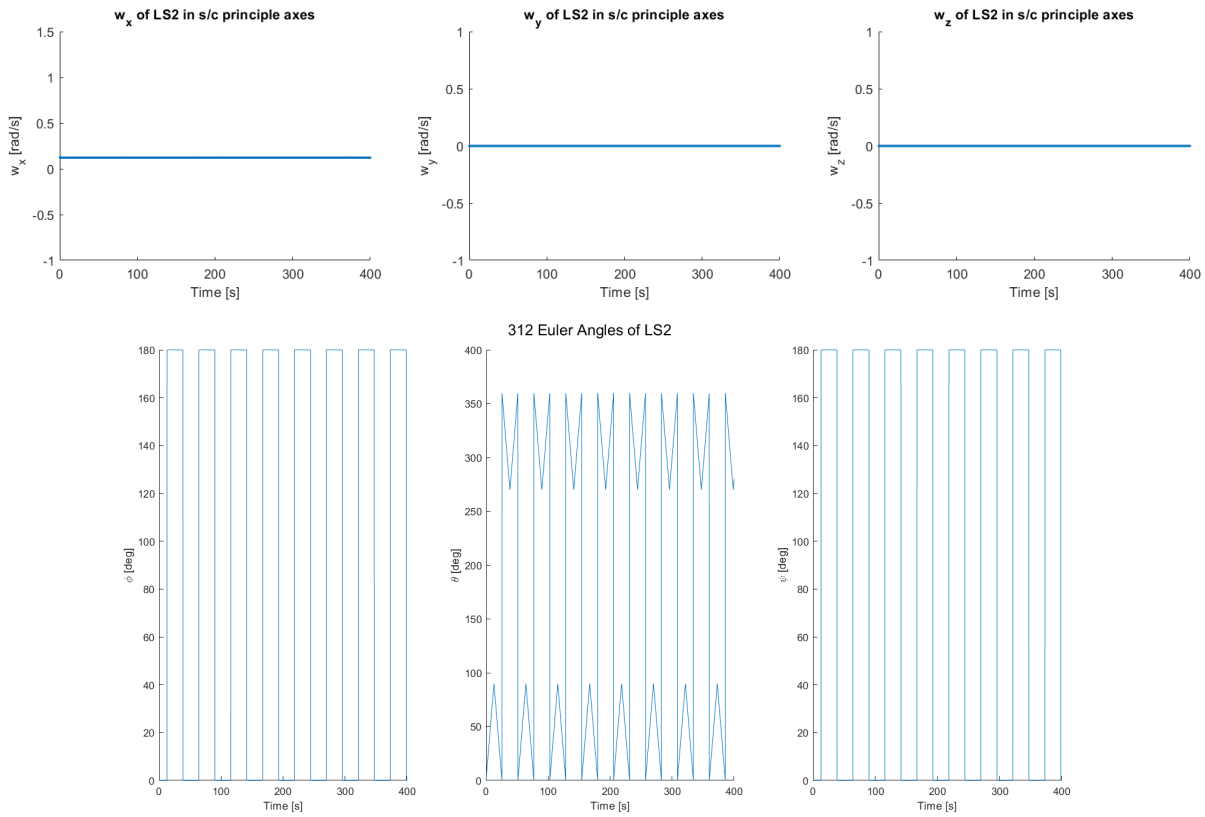


Figure 33: Dual spin equilibrium test with initial spin around X axis.

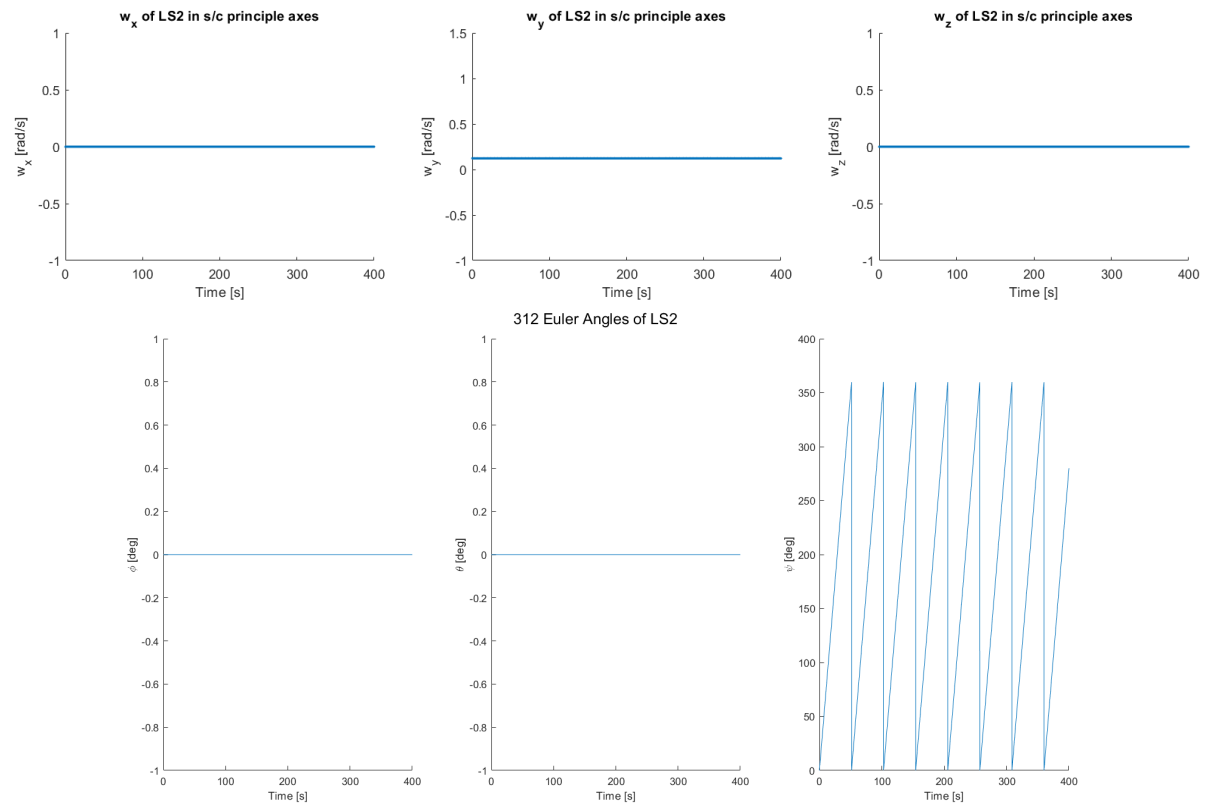


Figure 34: Dual spin equilibrium test with initial spin around Y axis.

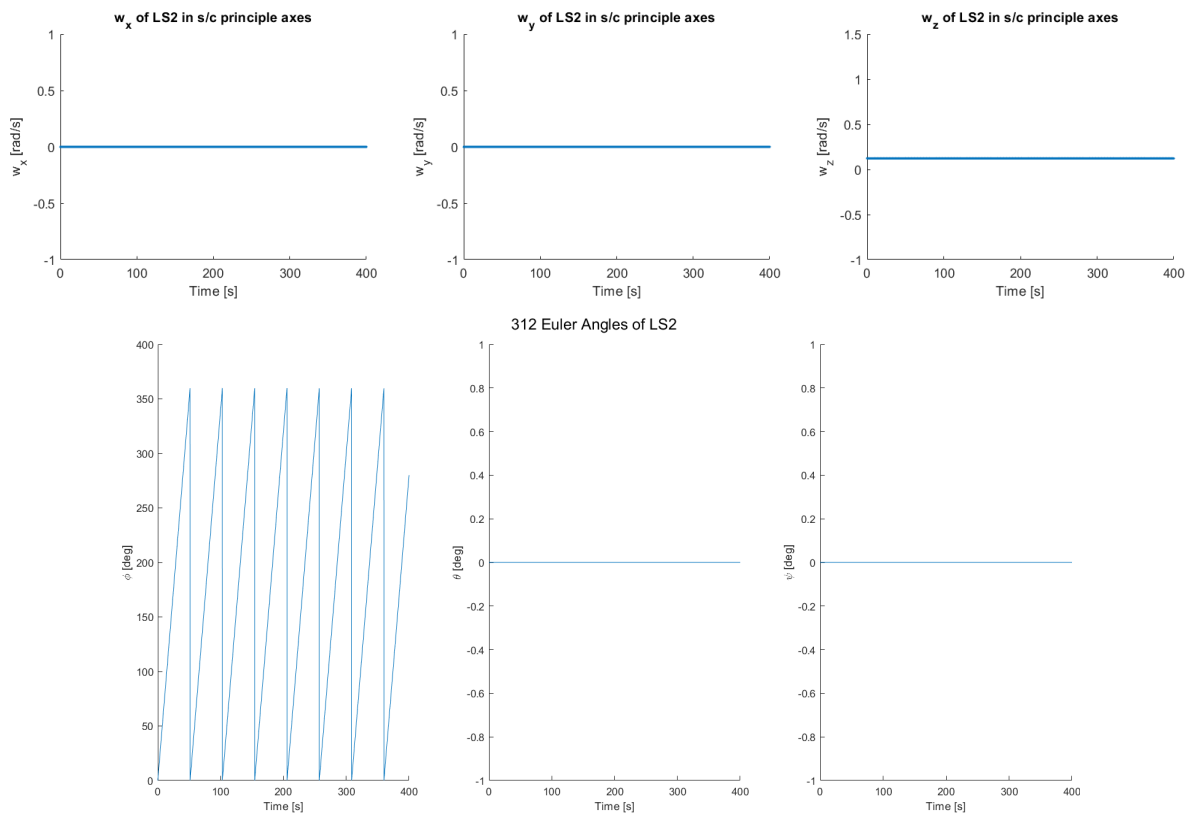


Figure 35: Dual spin equilibrium test with initial spin around Z axis.

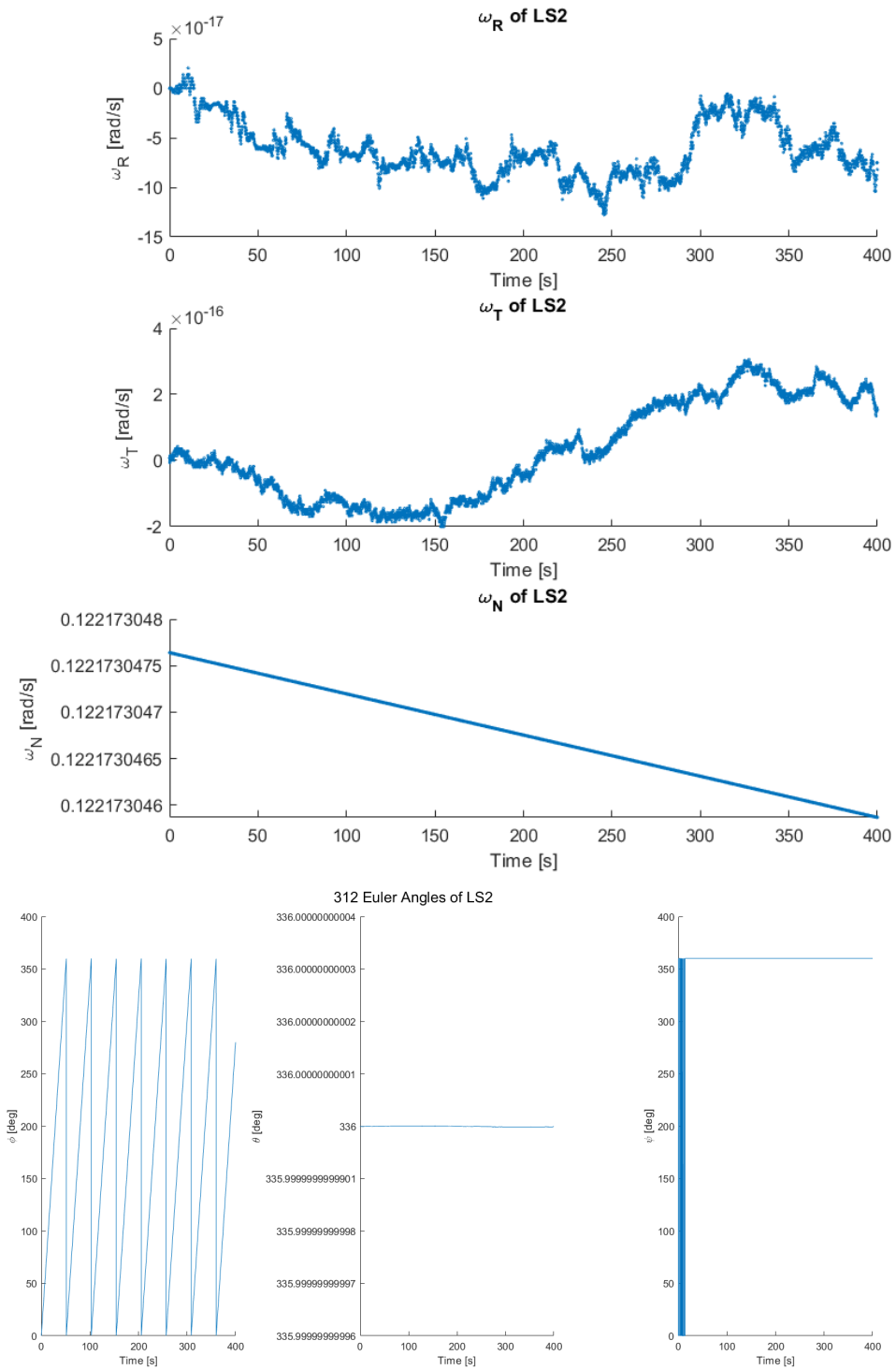


Figure 36: Dual spin equilibrium test with principal axes aligned with RTN, initial spin around N axis.

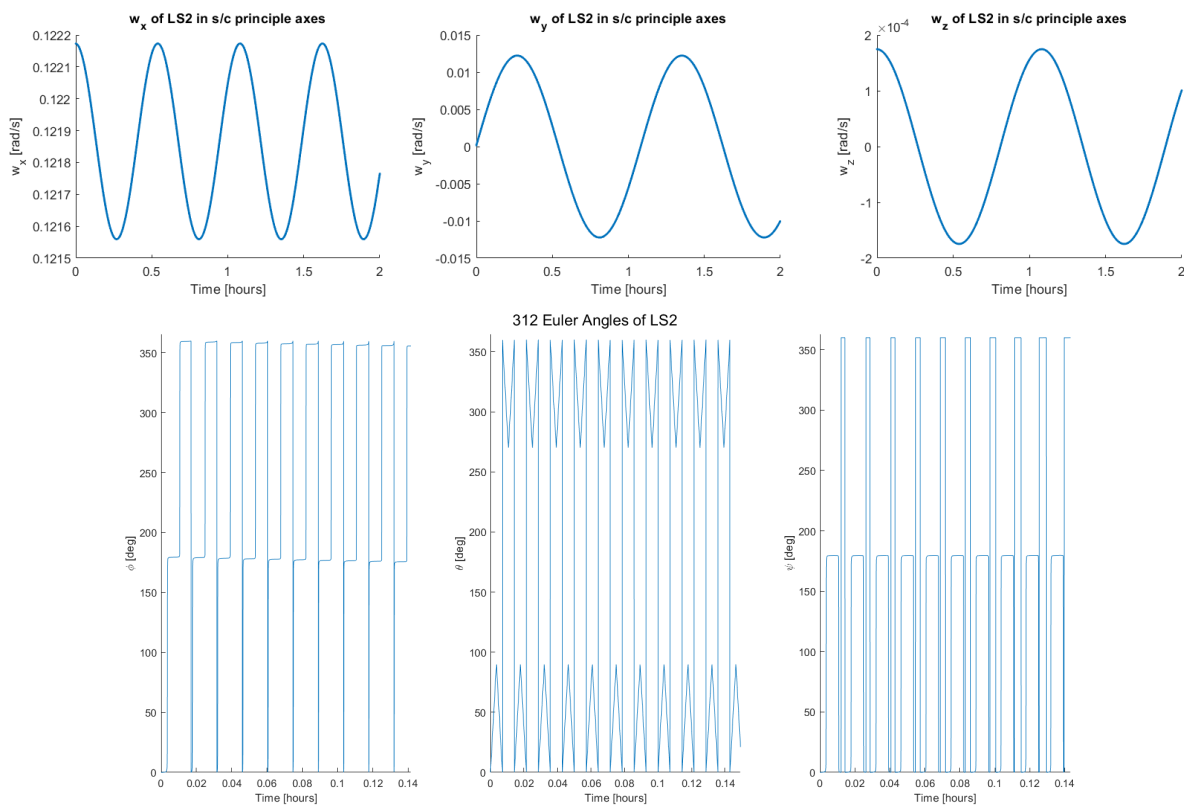


Figure 37: Dual spin stability test with initial spin mostly around X axis.

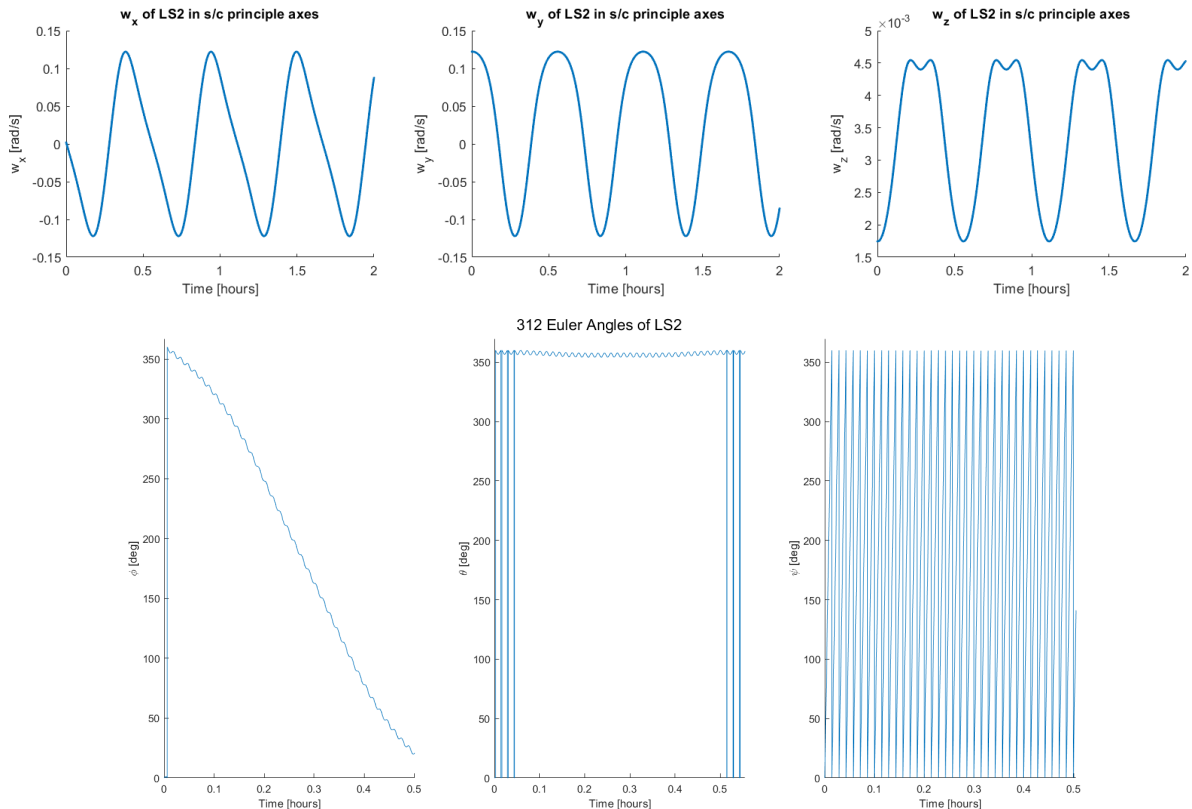


Figure 38: Dual spin stability test with initial spin mostly around Y axis.

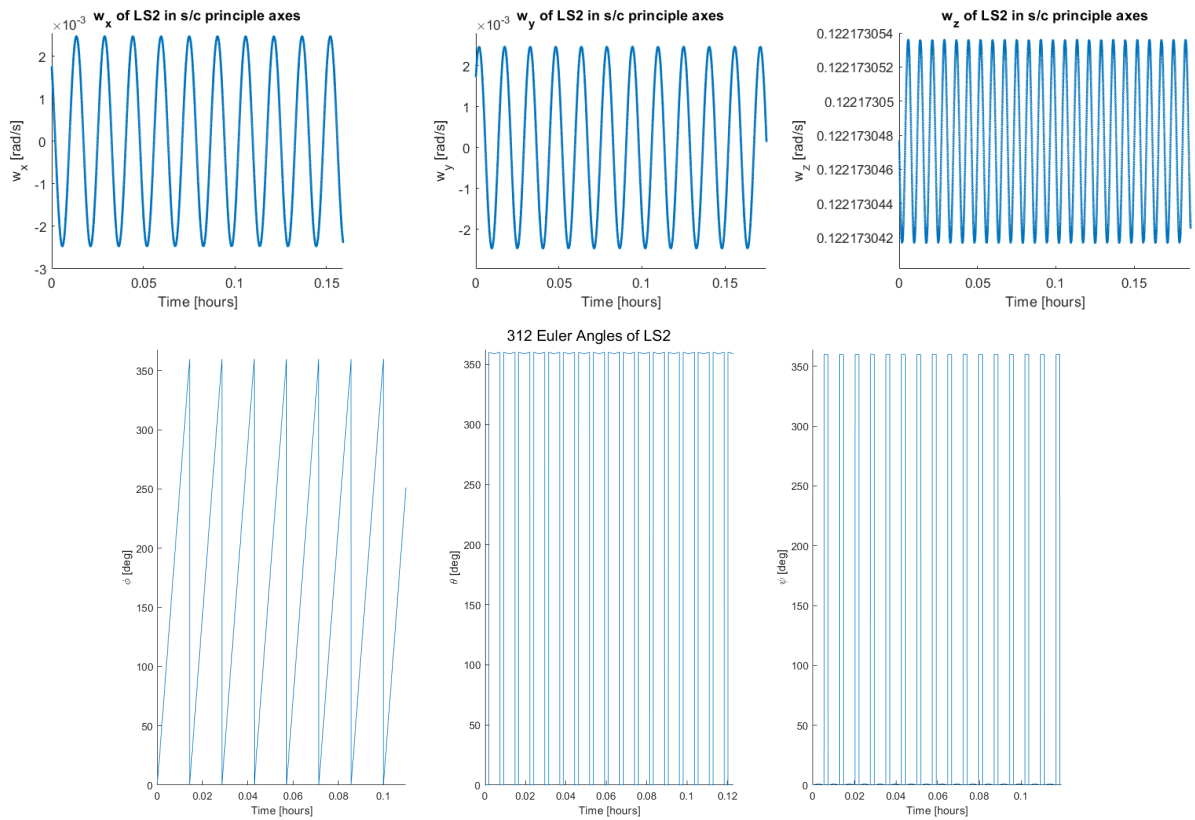


Figure 39: Dual spin stability test with initial spin mostly around Z axis.